Chapter 6: *Nowcasting* – Authors: Rita D. Roberts and James W. Wilson

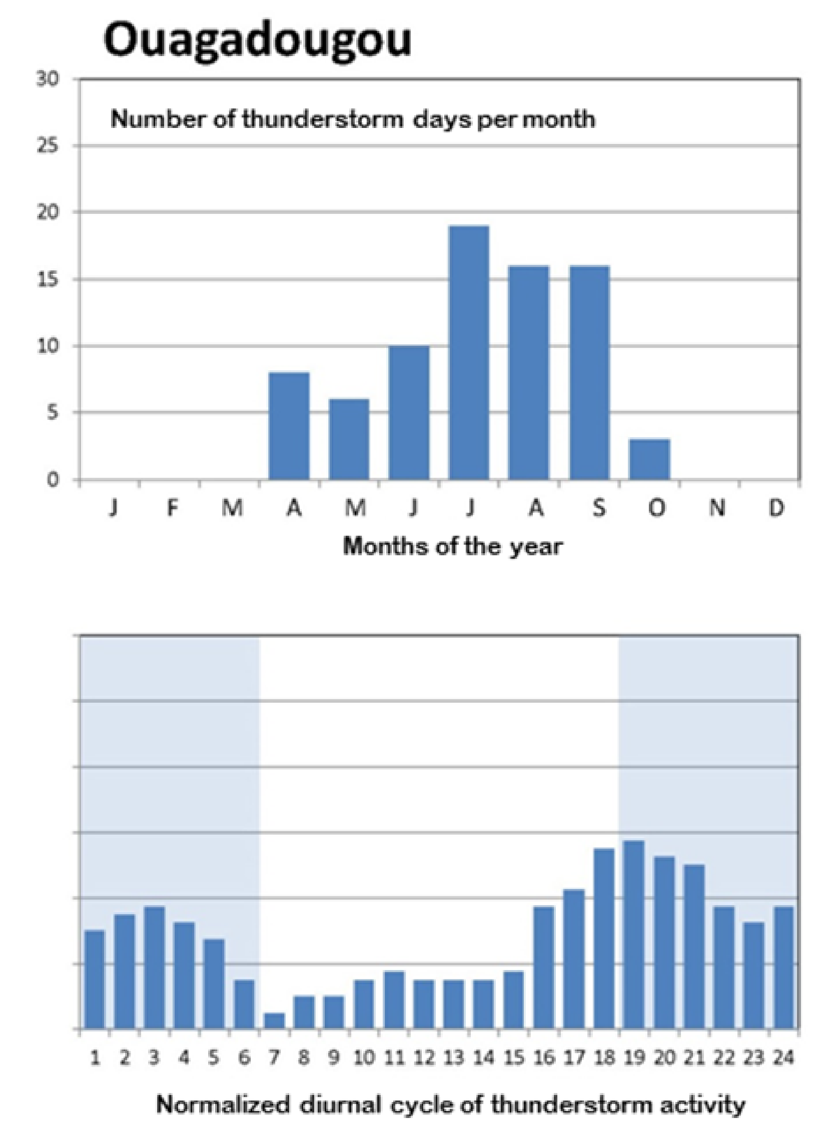

Figure 6.1. A climatology of all thunderstorms occurring in the vicinity of the Ouagadougou, Burkina Faso airport during 2012, showing the frequency of thunderstorms a) monthly and b) diurnally. (Source: Johnson et al., 2014)

Copyright © 2016 John Wiley & Sons

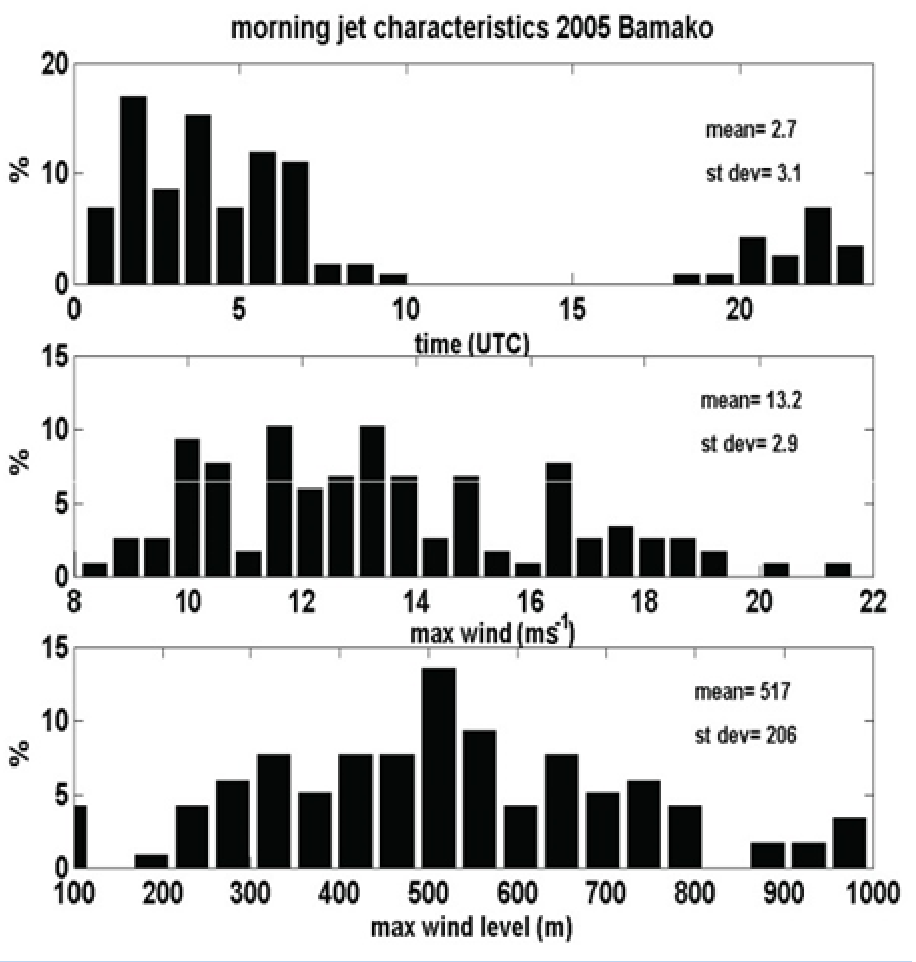

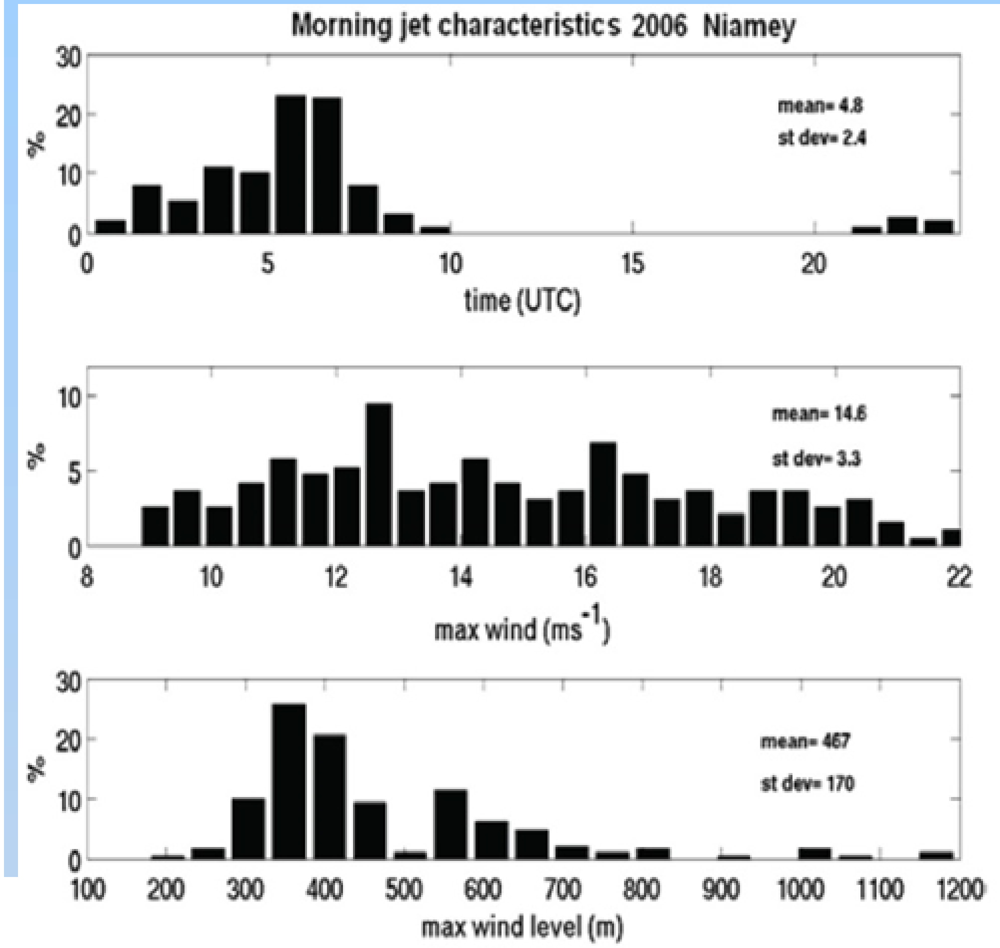

Figure 6.2. Characteristics of the nocturnal low-level jets in Bamako and Niamey. (Source: Madougou, 2010). See also Figure 4.11.

Copyright © 2016 John Wiley & Sons

Meteorology of Tropical West Africa: The Forecasters’ Handbook

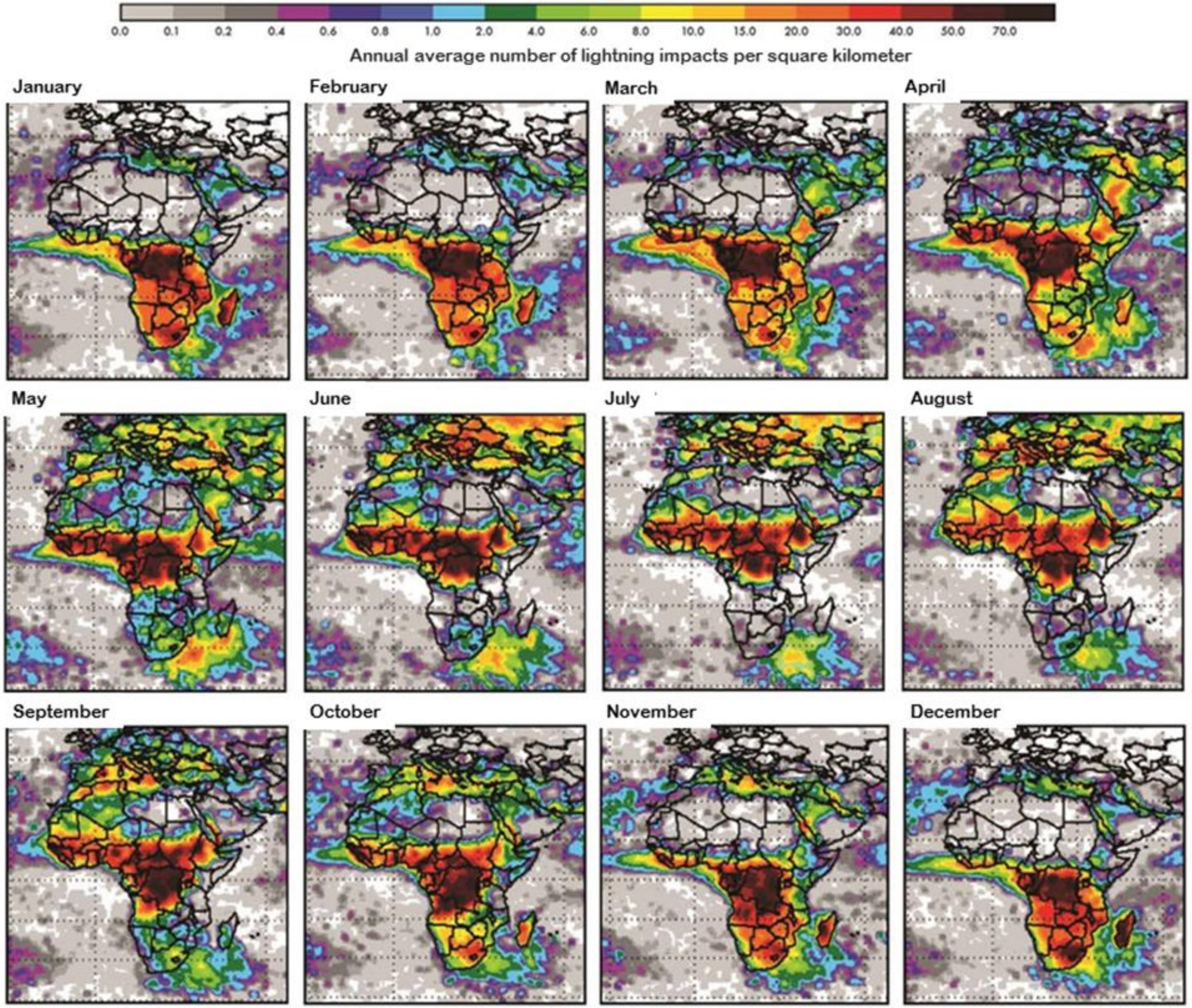

Figure 6.3. Monthly lightning climatologies for Africa produced from a decade of total lightning flash rates collected on NASA’s polar-orbiting satellites (Source: Johnson et al., 2014).

Copyright © 2016 John Wiley & Sons

Chapter 6: *Nowcasting* – Authors: Rita D. Roberts and James W. Wilson

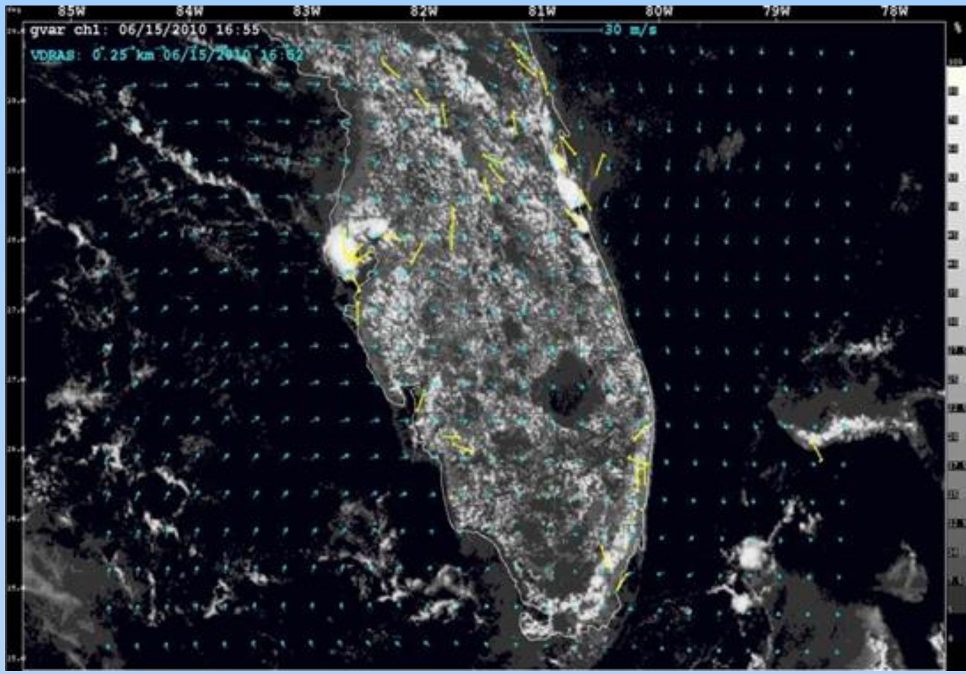

Figure 6.4. High-resolution, gridded climatology used in nowcasting convective storms for the Florida peninsula in the U.S.A. Top panel: satellite visible imagery of convective storm development at 1700 UTC (13:00 LT). Bottom panel: Seven years, climatology of lightning frequency on a 1-km resolution grid, valid for the same time period indicating locations of highest frequency of thunderstorms.
(Source: R. Roberts, 2014)

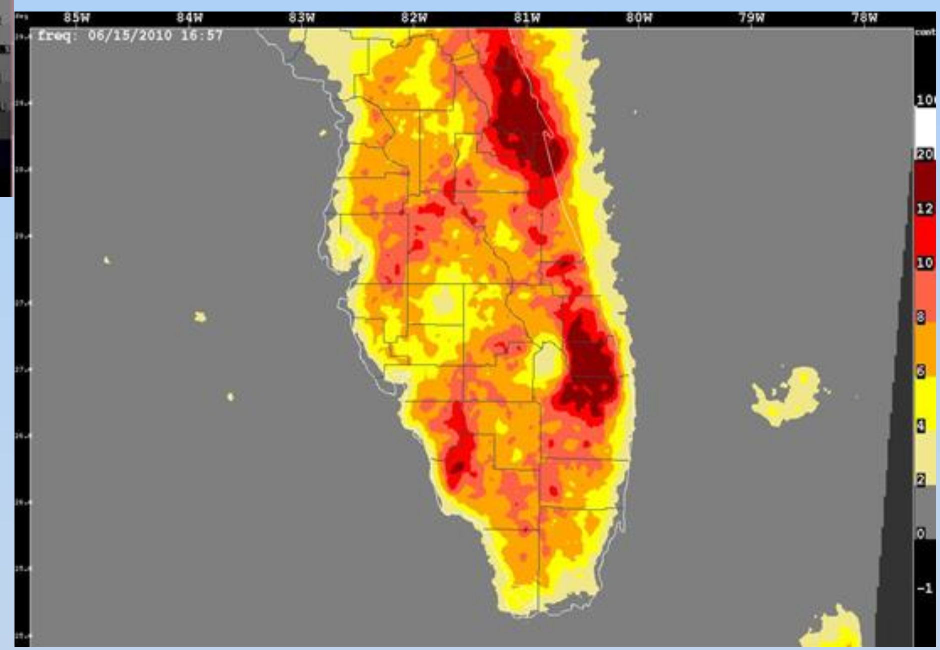

Copyright © 2016 John Wiley & Sons

Chapter 6: *Nowcasting* – Authors: Rita D. Roberts and James W. Wilson

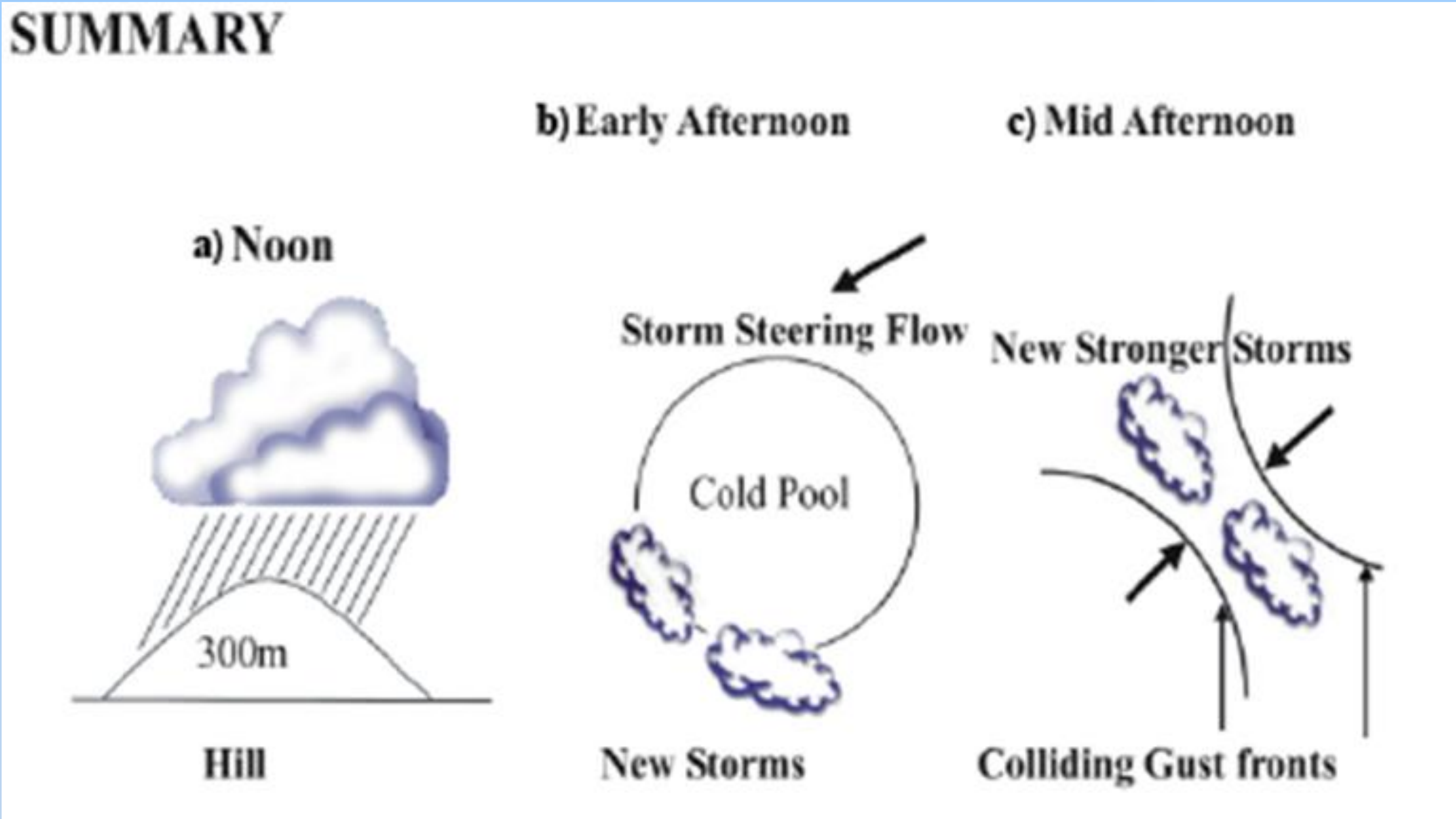

Figure 6.5. Conceptual model of storm initiation and evolution over the Amazon River Basin (Source: Lima and Wilson, 2008). See text for explanation.

Copyright © 2016 John Wiley & Sons

Chapter 6: *Nowcasting* – Authors: Rita D. Roberts and James W. Wilson

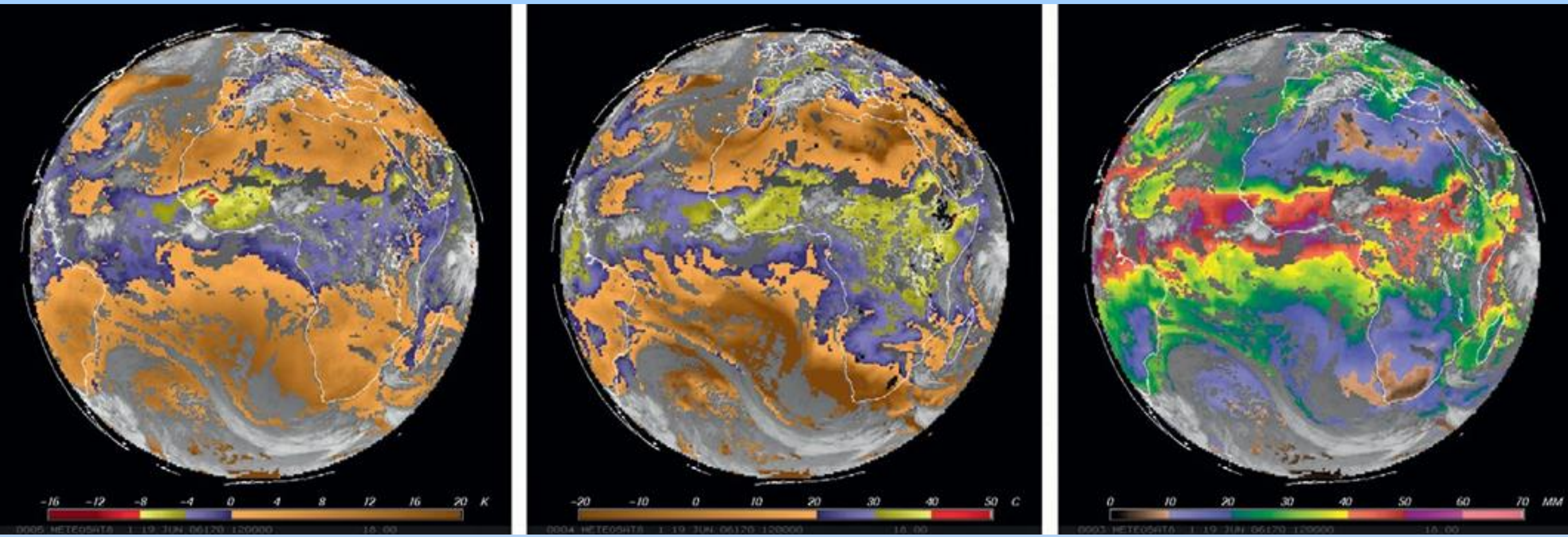

Figure 6.6. Examples of the EUMETSAT Global Instability Index products derived from the MSG satellite for Africa on 19 June 2006. Indices shown in the panels are: lifted index (left), K index (centre) and Total Precipitable Water (right). (Source: Koenig and de Coning, 2009.)

Copyright © 2016 John Wiley & Sons

African Monsoon Multidisciplinary Analysis

ACMAD

WMO

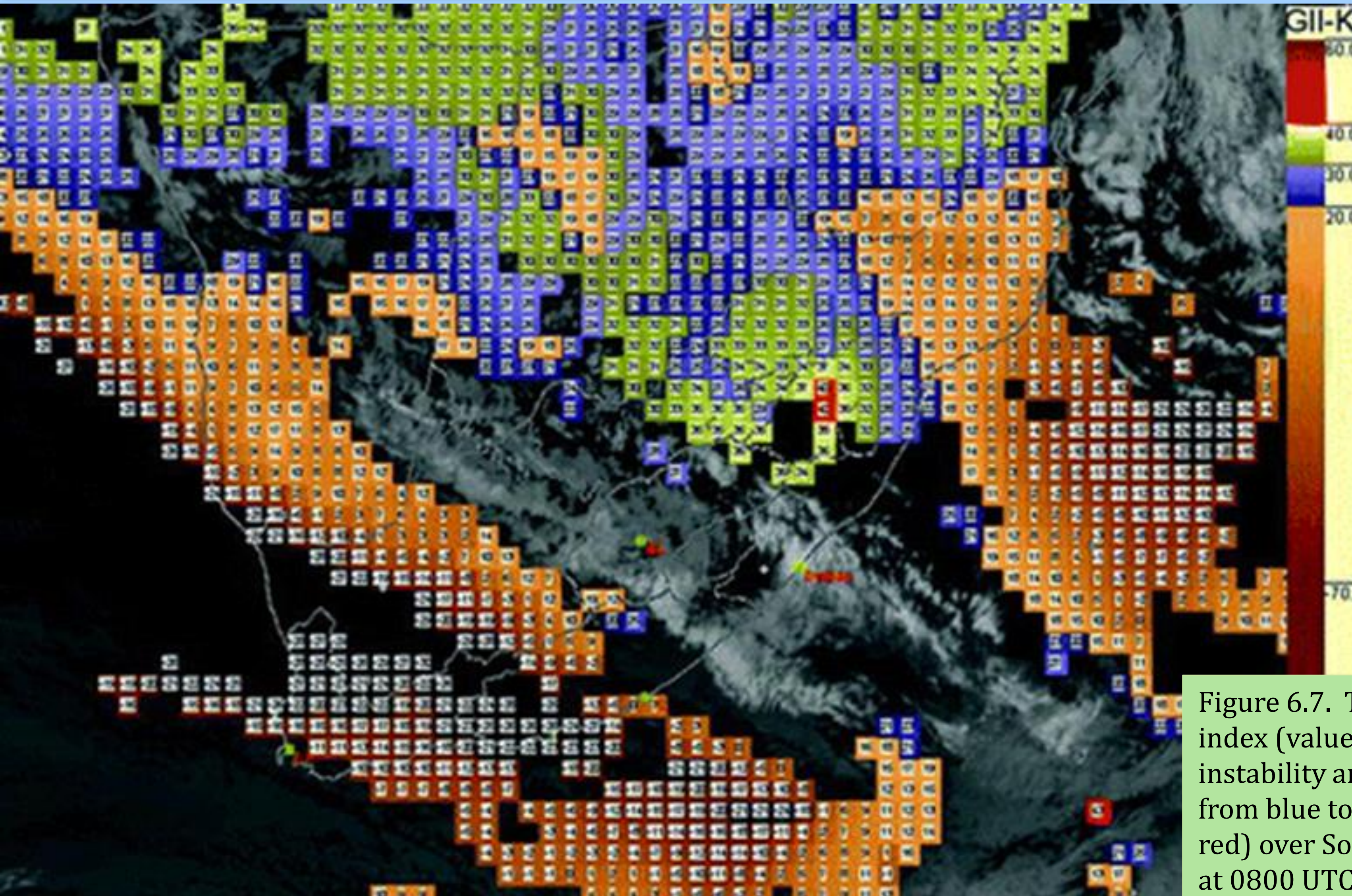

Figure 6.7. The K index (values of instability are shown from blue to yellow to red) over South Africa, at 0800 UTC 26 Oct 2006.

Copyright © 2016 John Wiley & Sons

Chapter 6: *Nowcasting* – Authors: Rita D. Roberts and James W. Wilson

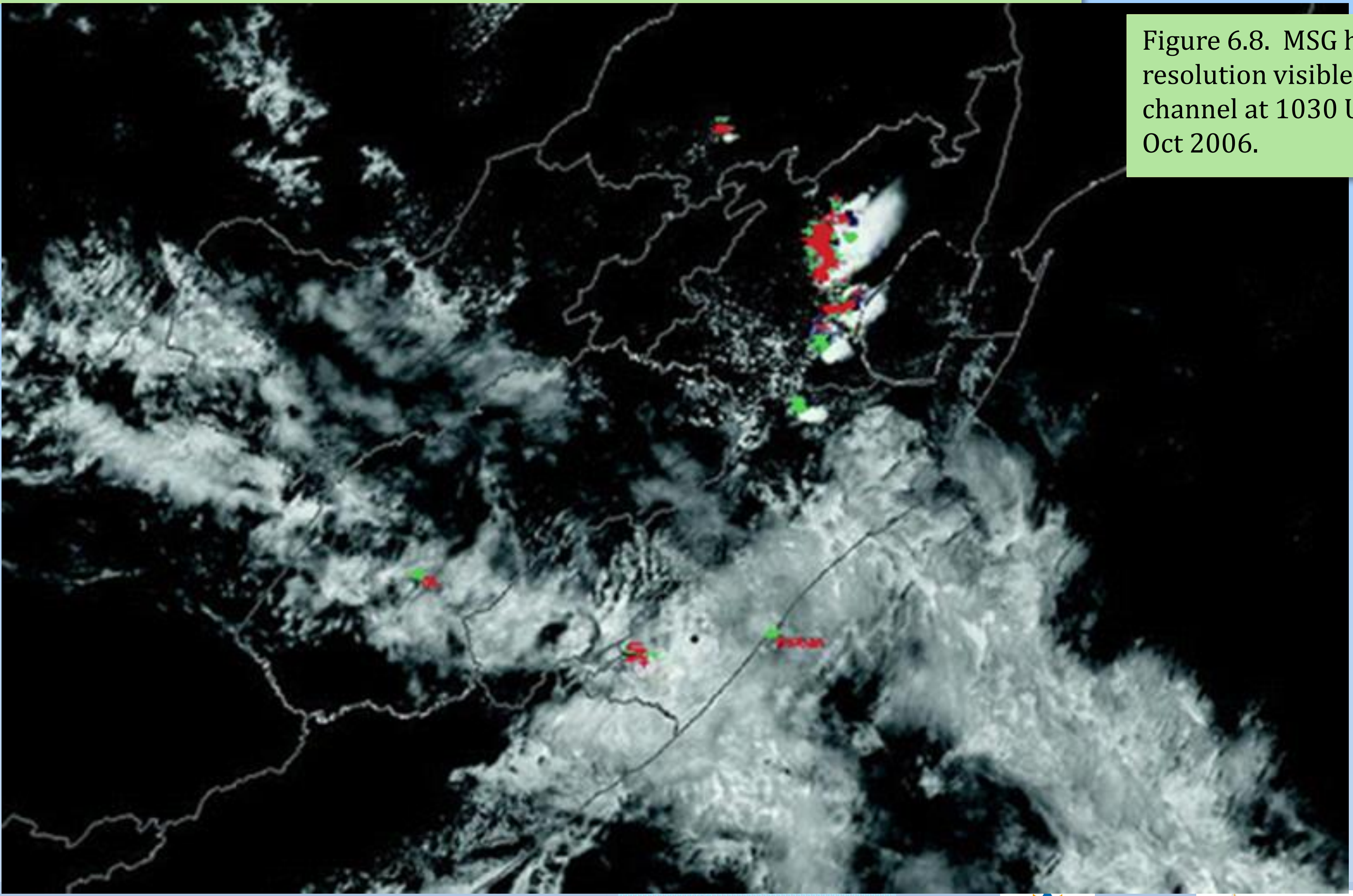

Figure 6.8. MSG high-resolution visible (HRV) channel at 1030 UTC 26 Oct 2006.

Copyright © 2016 John Wiley & Sons

African Monsoon Multidisciplinary Analysis

ACMAD

WMO

Chapter 6: *Nowcasting* – Authors: Rita D. Roberts and James W. Wilson

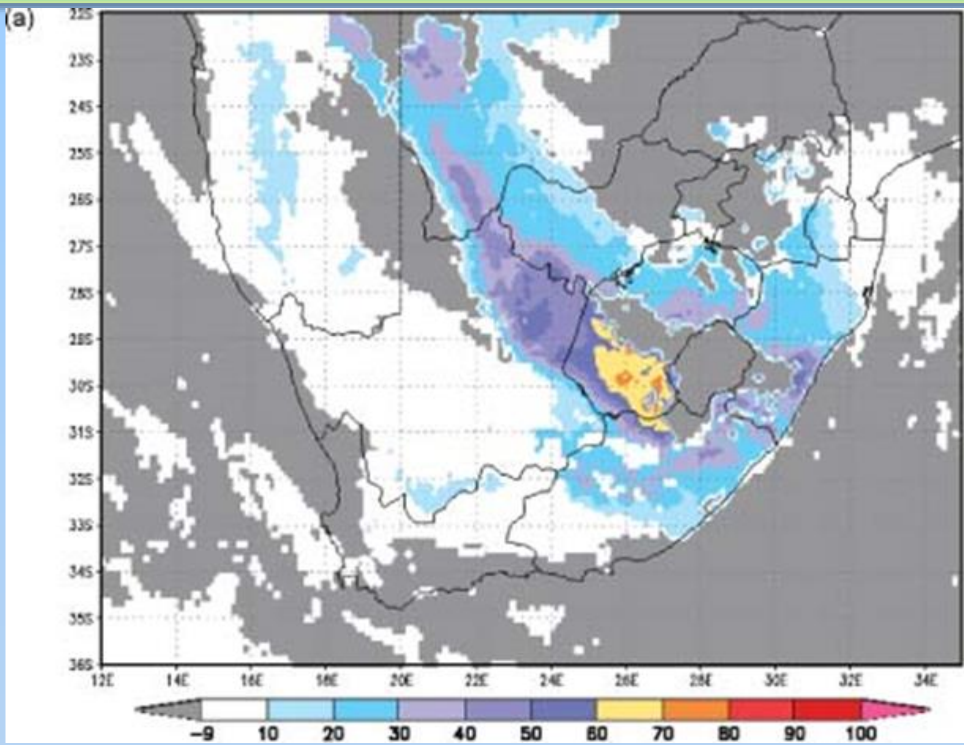

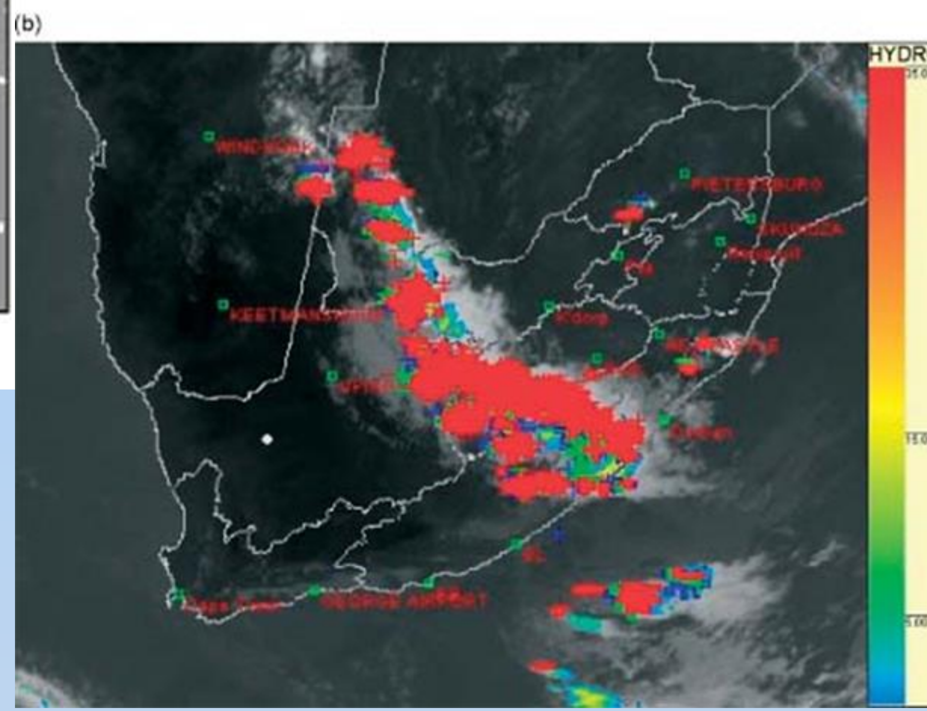

Figure 6.9. Three-hourly time average of CII between 0600 and 0900 UTC (%) over South Africa (a) and lightning occurrence (indicated in red, green, and blue crossed) as well as Hydroestimator (mm) at 1500 UTC (b) for 31 January 2010. Grey shading indicated cloud cover. (Source: de Coning et al., 2011;

Copyright © 2016 John Wiley & Sons

Chapter 6: *Nowcasting* – Authors: Rita D. Roberts and James W. Wilson

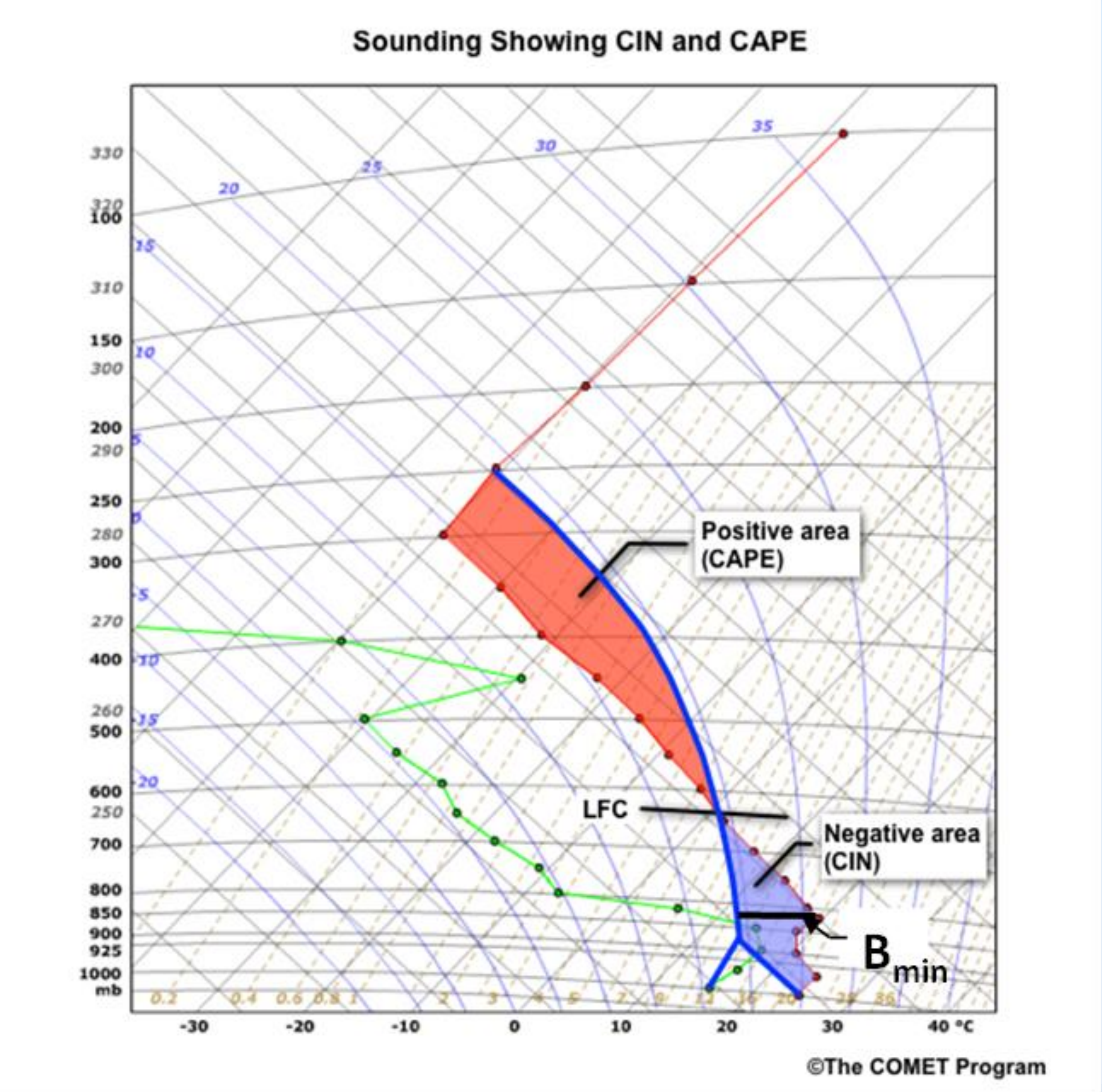

Figure 6.10. Example tephigram sounding for a given day and time, showing the negative and positively buoyant areas of the atmosphere for a parcel being lifted from the surface.

Copyright © 2016 John Wiley & Sons

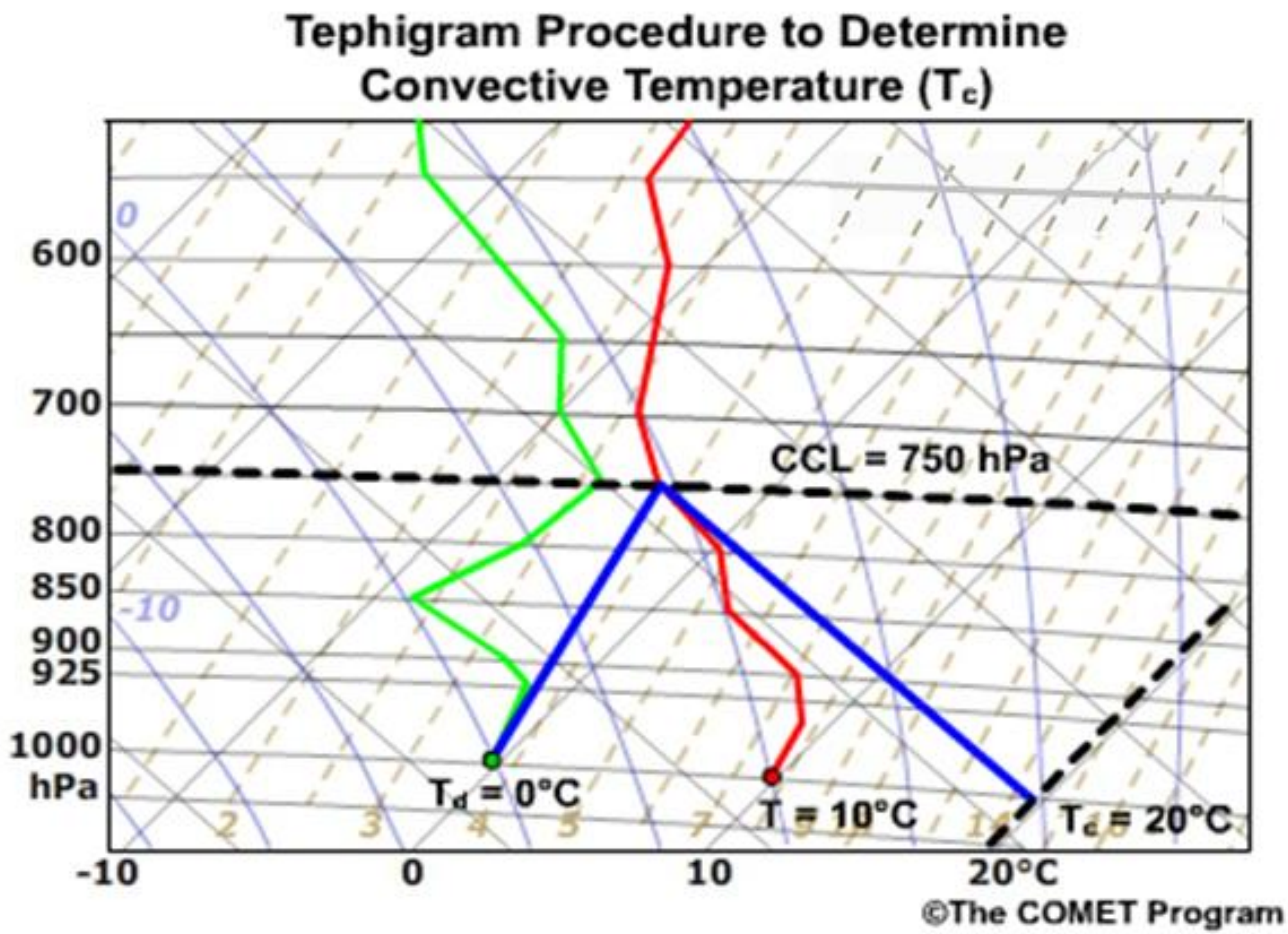

Figure 6.11. Process for computing Convective Temperature.

Copyright © 2016 John Wiley & Sons

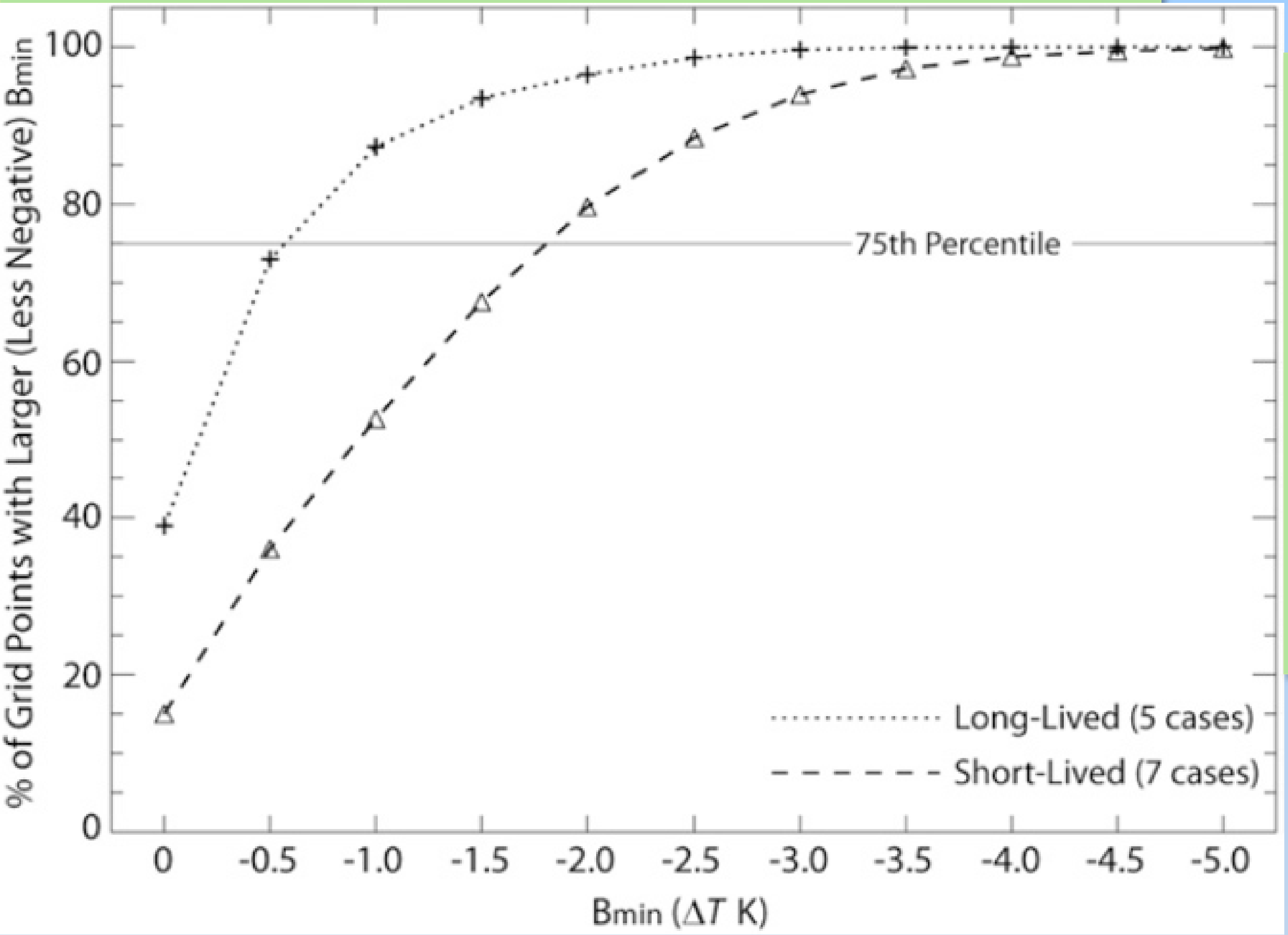

Figure 6.12. Cumulative distribution functions for minimum negative buoyancy for the most unstable parcel over a 400 x 400 km2 grid region for the long- and short-lived simulated cases at 1200 UTC (Source: Laing et al., 2012;

Copyright © 2016 John Wiley & Sons

Chapter 6: *Nowcasting* – Authors: Rita D. Roberts and James W. Wilson

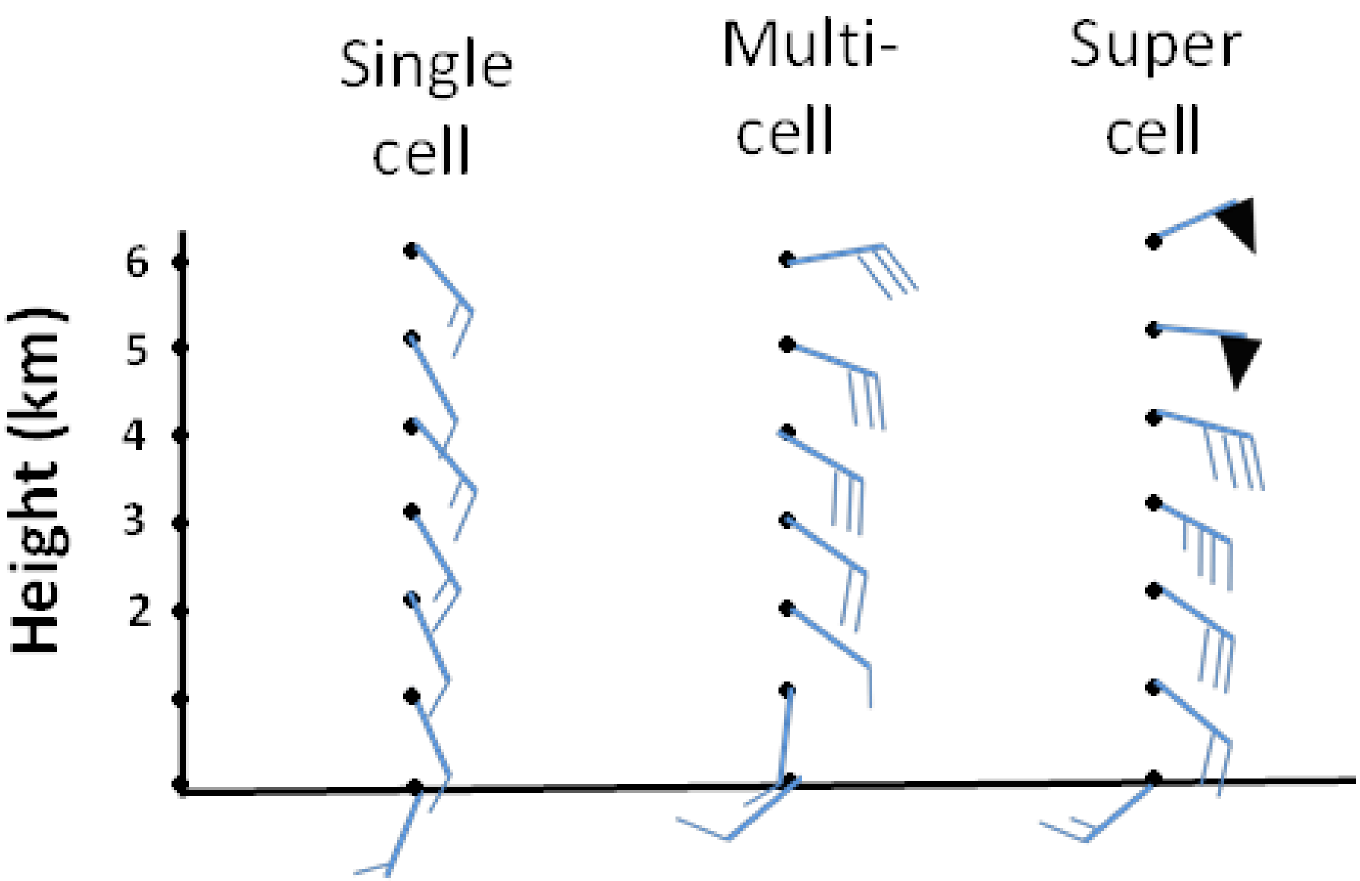

Figure 6.13. Proposed sample vertical wind shear profiles for single cell, multi-cell and super cell storms for West Africa. The multi-cell storm is characterised by much stronger rotational shear of the winds. These are educated guesses based on North American studies and the reader should note that there is little or no evidence of supercell storms occurring in West Africa. A half barb is 5 knots, full barb is 10 knots and a flag is 50 knots. (Source: J. Wilson, 2014)

Copyright © 2016 John Wiley & Sons

African Monsoon Multidisciplinary Analysis

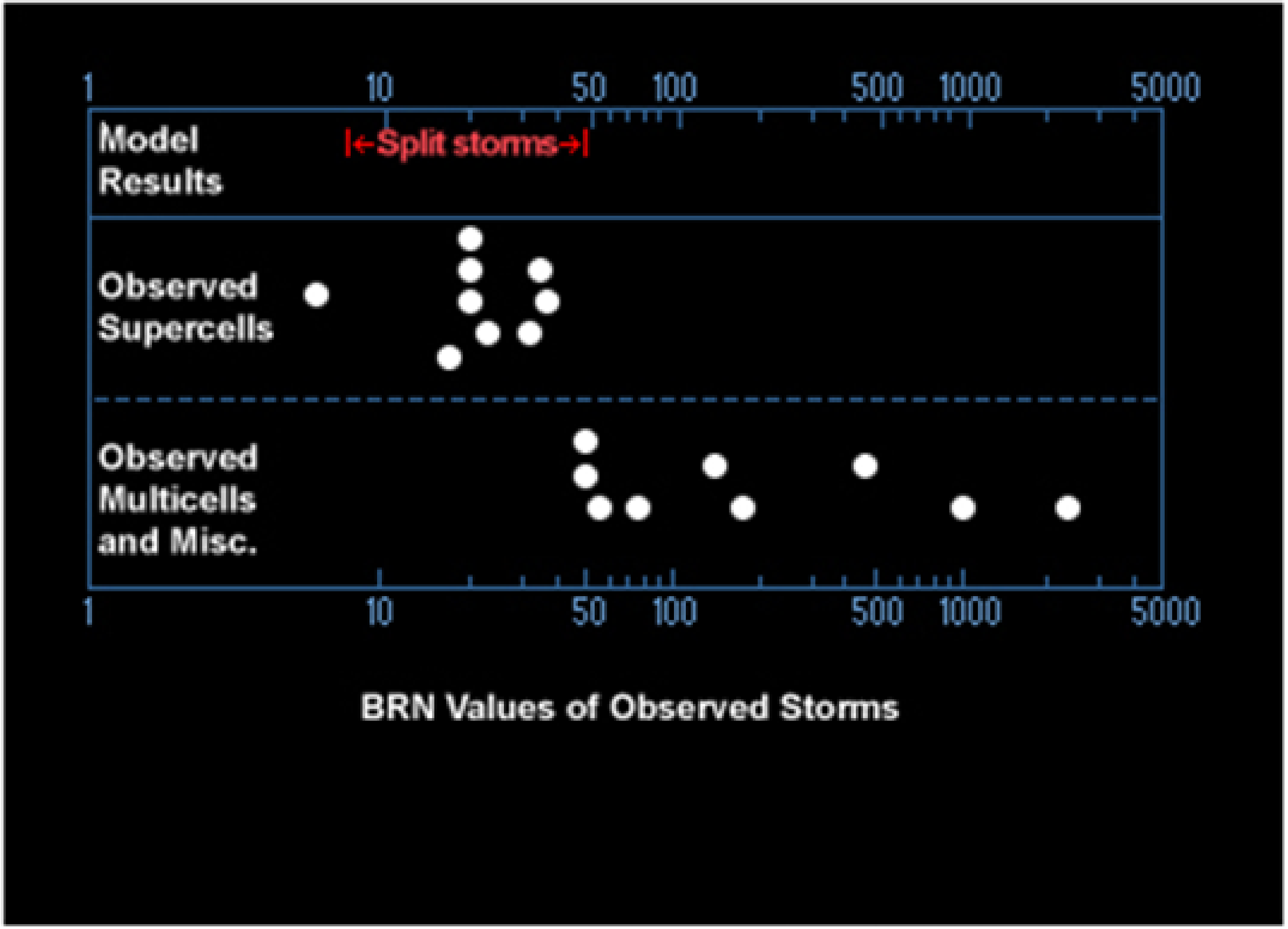

Adapted from Weisman and Klemp, 1982

Figure .6.14. Types of observed storms for different bulk Richardson (BRN) values derived from NWP model-retrieved soundings. (Source: The COMET Program)

Copyright © 2016 John Wiley & Sons

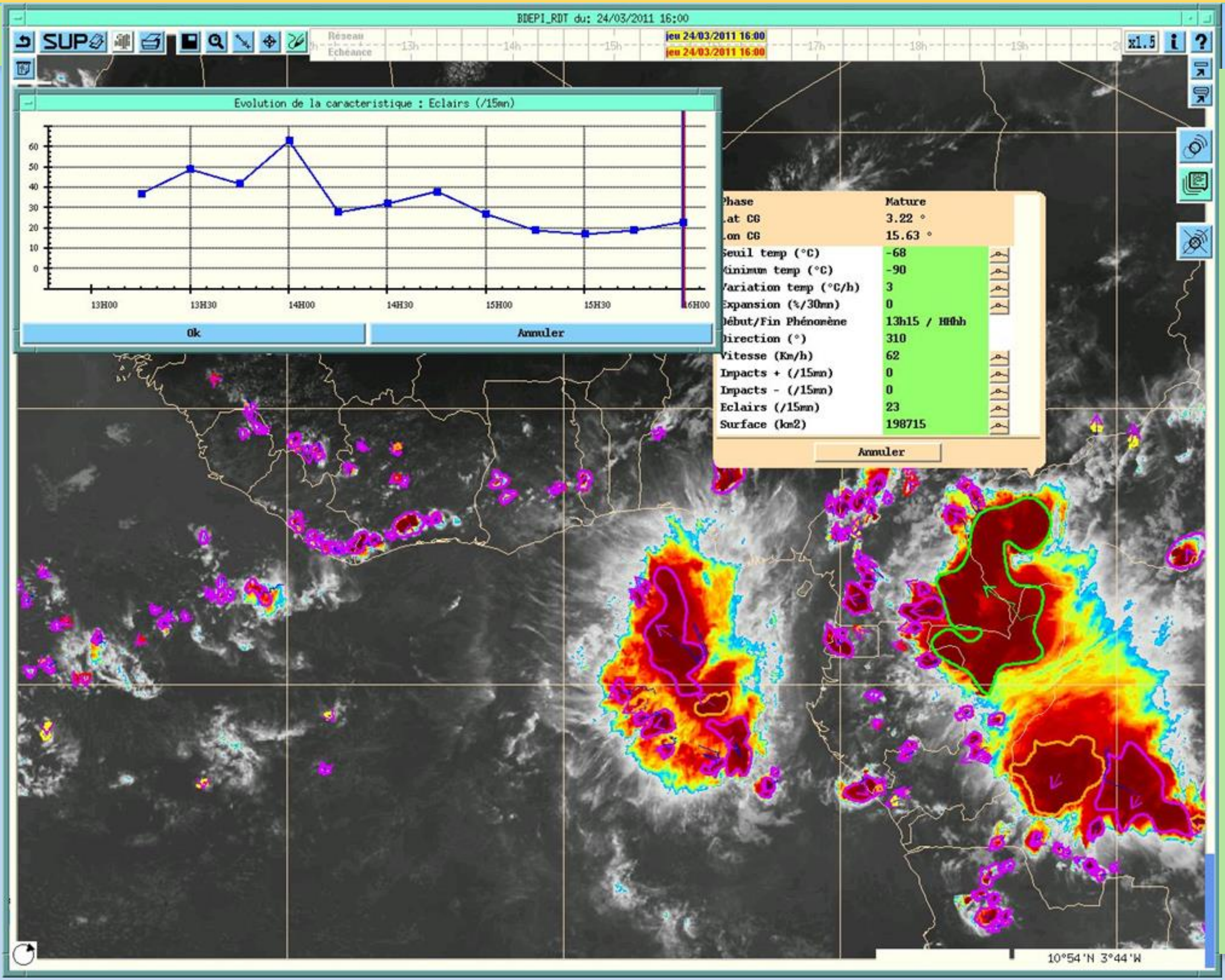

Figure 6.15. Example of the Rapid Development Thunderstorm (RDT) Product for West Africa for tracking storms observed in satellite data. Coloured polygons and vectors overlaid on satellite imagery are automated storm detection and motion products. Specific information on storm and lightning characteristics and storm motion for the storm bounded by a green polygon are shown in the pop-up window. (Source: Météo-France web site; 2014.)

Copyright © 2016 John Wiley & Sons

Chapter 6: *Nowcasting* – Authors: Rita D. Roberts and James W. Wilson

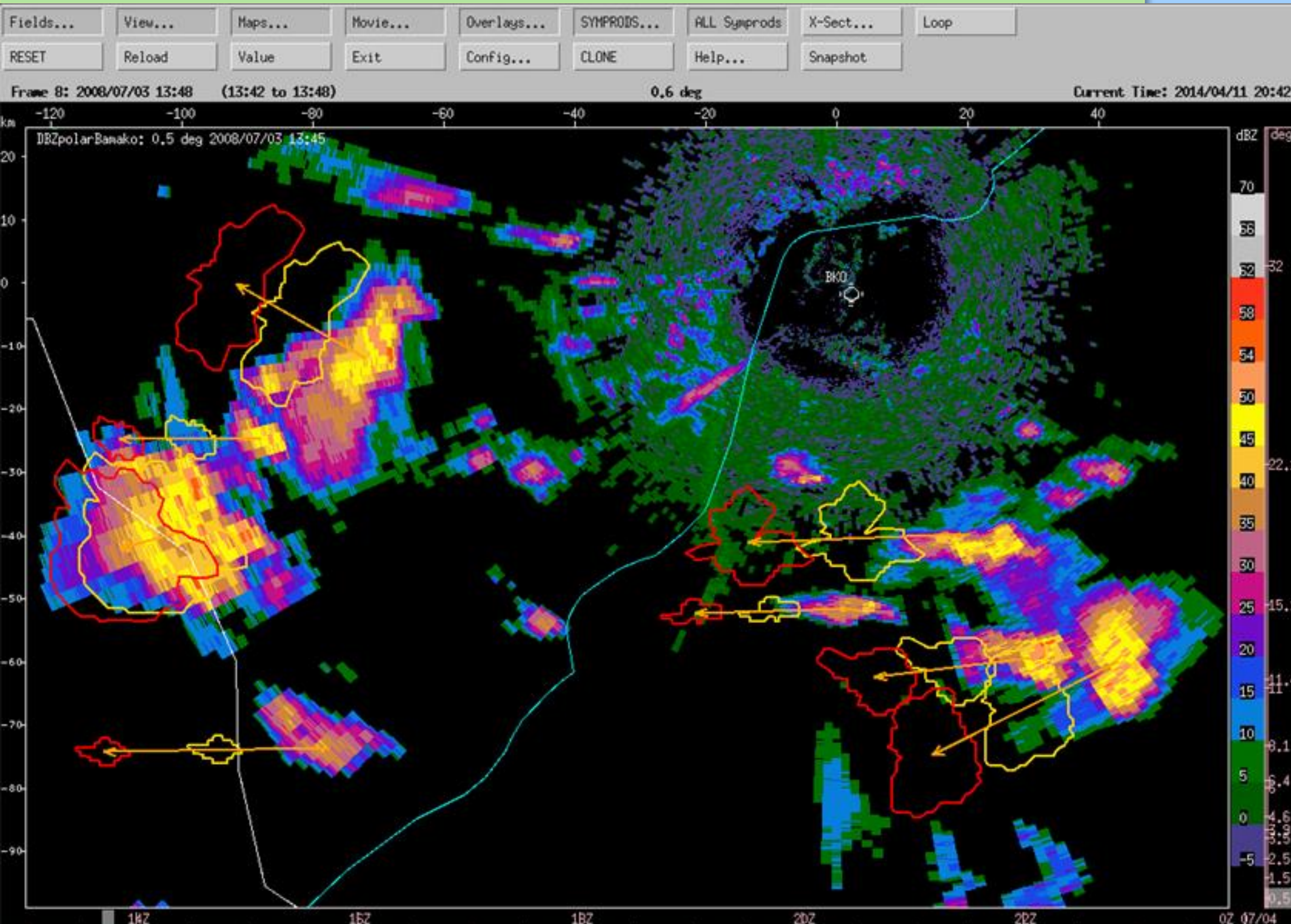

Figure 6. 16. Example of automated storm extrapolations run on radar data from Bamako, Mali using the TITAN algorithm (Dixon and Wiener, 1993). Shown are 30-min (orange polygons) and 60-min (red polygons) storm extrapolations and the storm motion vectors on 3 July 2008. Blue contour is the Niger River. Bamako-Senou International Airport is located at x=3km, y = -2km. (Source: R. Roberts, 2014)

Copyright © 2016 John Wiley & Sons

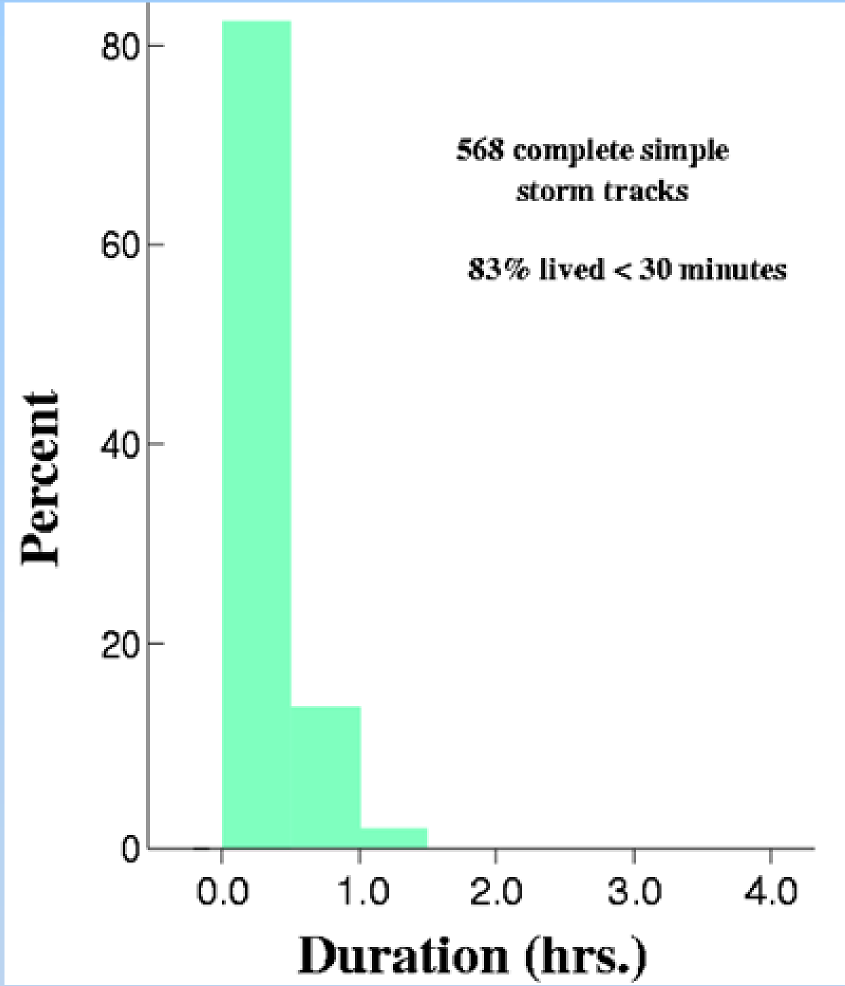

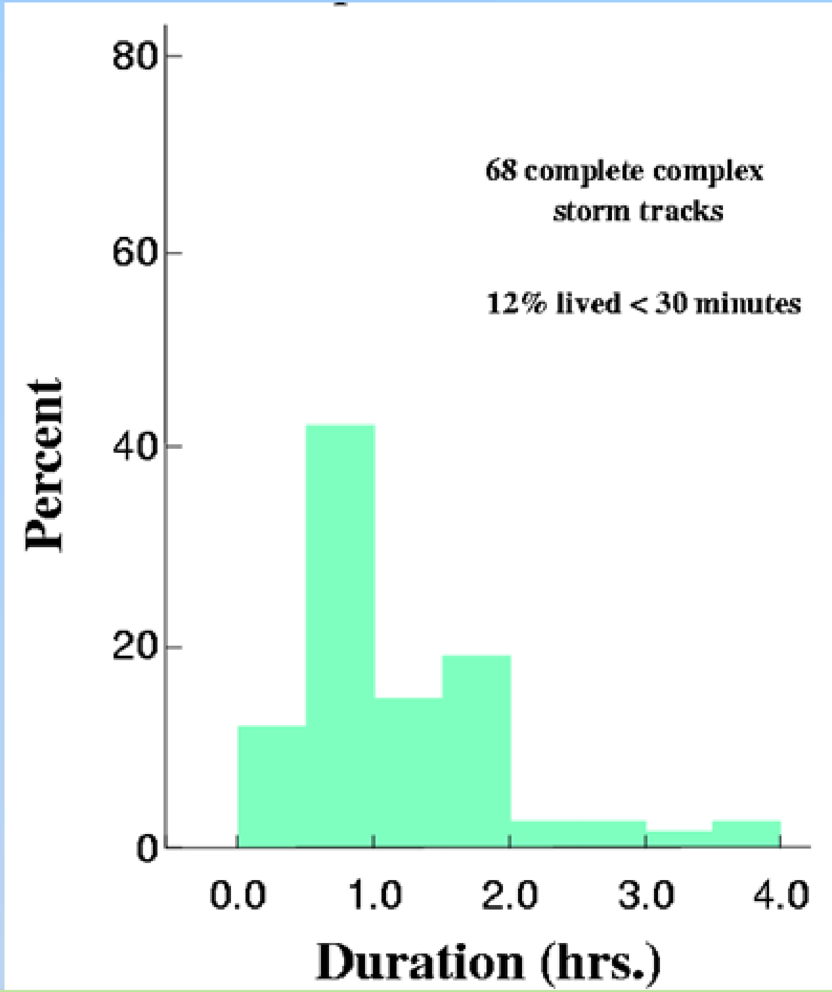

Figure 6.17. Histogram showing the lifetime of simple and complex storms observed during the summer of 1991 near Denver, Colorado (U.S.A.), based on data from an automated cell tracking system called TITAN. A simple storm is one that does not merge or split during its lifetime and complex storm is one that does. (Source: Henry, 1993).

Copyright © 2016 John Wiley & Sons

Chapter 6: *Nowcasting* – Authors: Rita D. Roberts and James W. Wilson

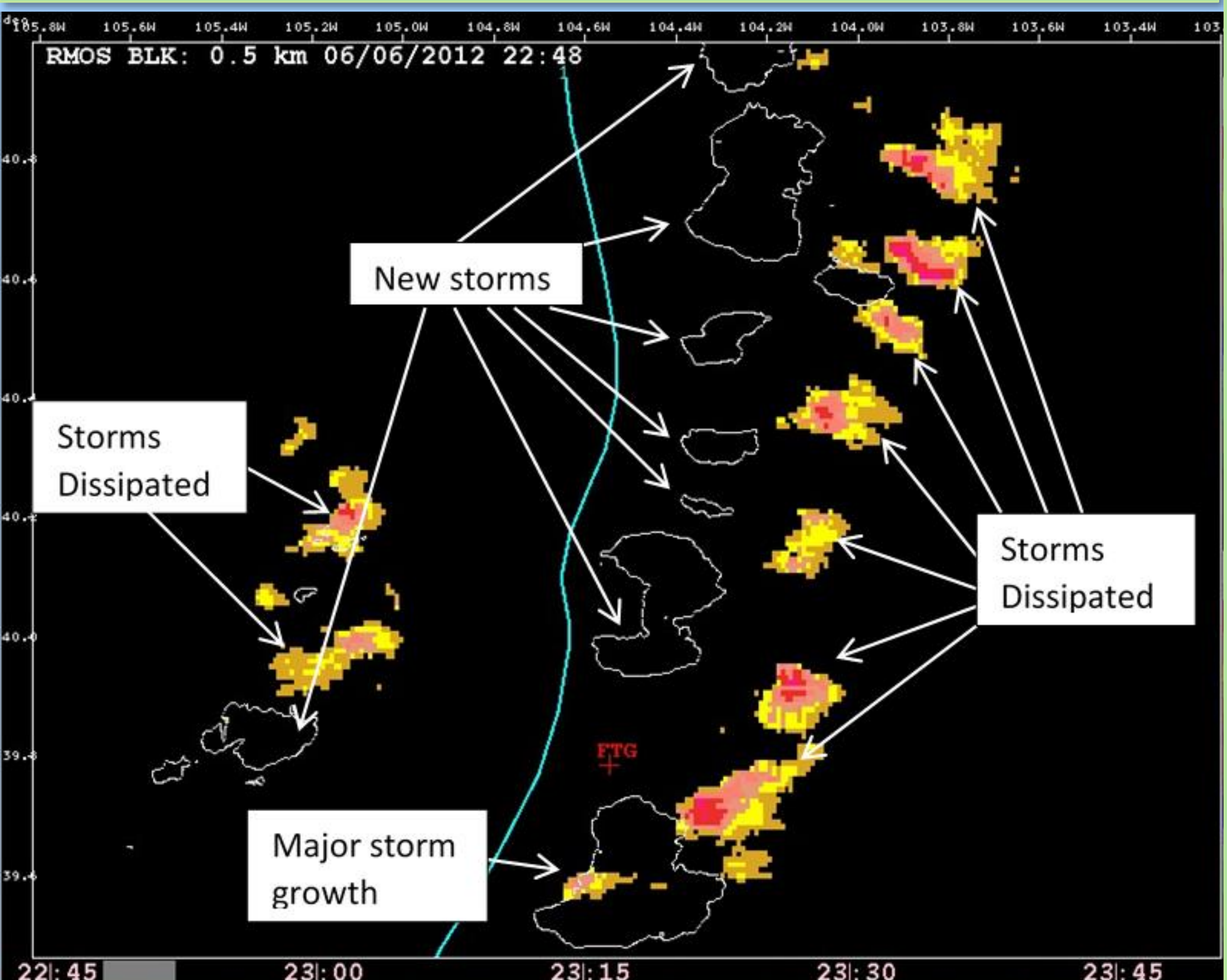

Figure 6.18. Sixty-minute extrapolation nowcast of storm position and intensity (colour filled objects) and actual location of storms at verification time (white contours). The outer colour is a radar reflectivity of 35 dBZ with each new colour increasing in 5 dBZ steps. The echoes were moving primarily from the southwest. The white contour is 35 dBZ. This is an extreme example where nearly all the extrapolated storms dissipated within 60 min even though many of the storms were > 50 dBZ. The N-S line of new storms are mostly > 50 dBZ that initiated just east of a boundary-layer convergence line (blue line). (Source: J. Wilson, 2014)

Copyright © 2016 John Wiley & Sons

Chapter 6: *Nowcasting* – Authors: Rita D. Roberts and James W. Wilson

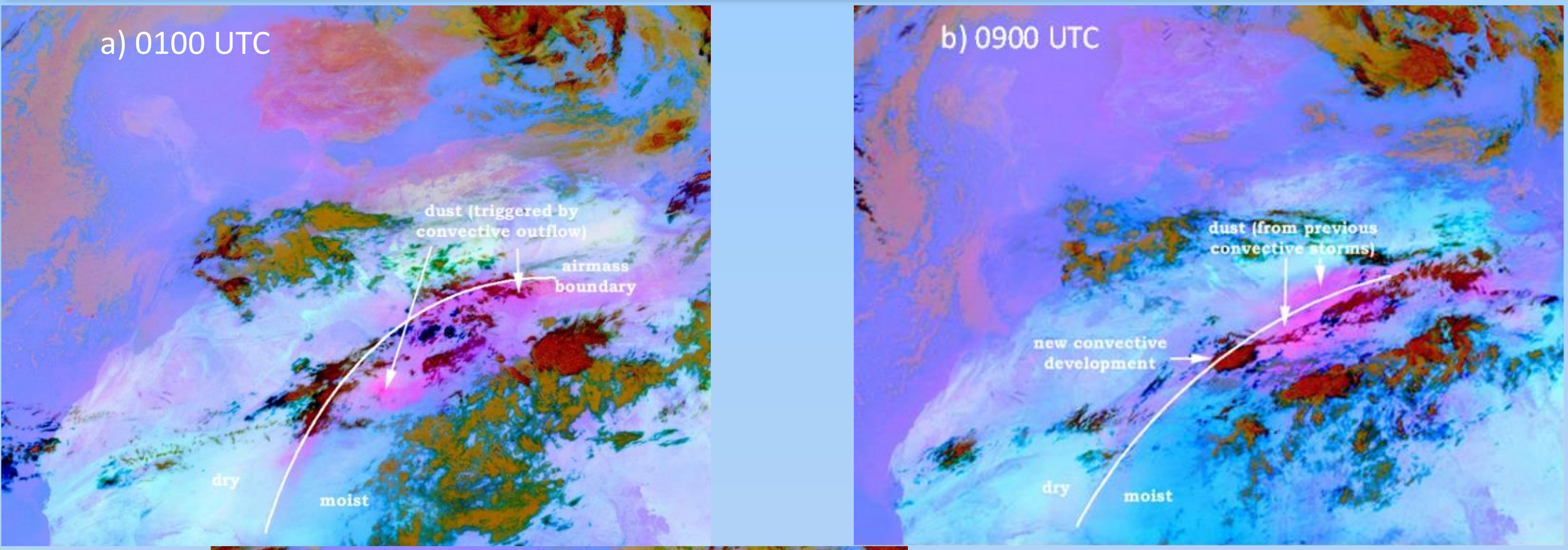

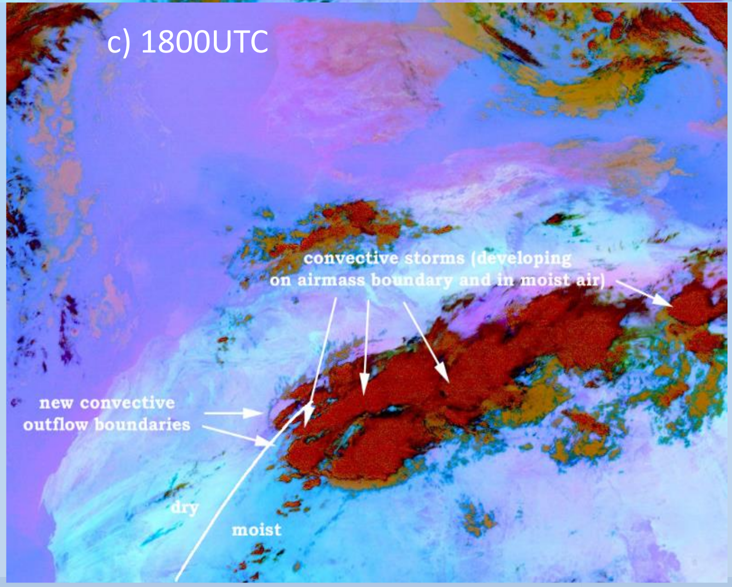

Figure 6.19. Dust RGB plots highlighting low-level convergence boundaries between moist and dry air and storm initiation and evolution above these boundaries on 4 October 2005 at three time periods. (Source: EUMETSAT web site; 2014)

Copyright © 2016 John Wiley & Sons
African Monsoon Multidisciplinary Analysis
ACMAD
WMO

Chapter 6: *Nowcasting* – Authors: Rita D. Roberts and James W. Wilson

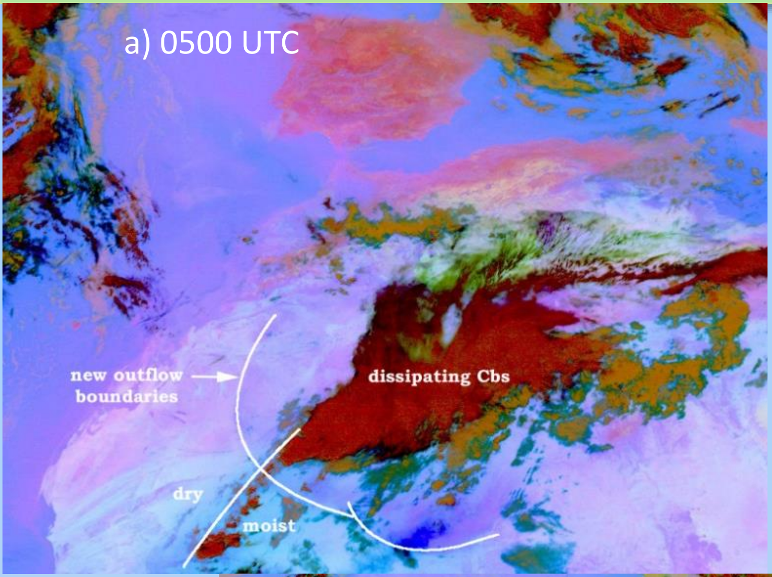

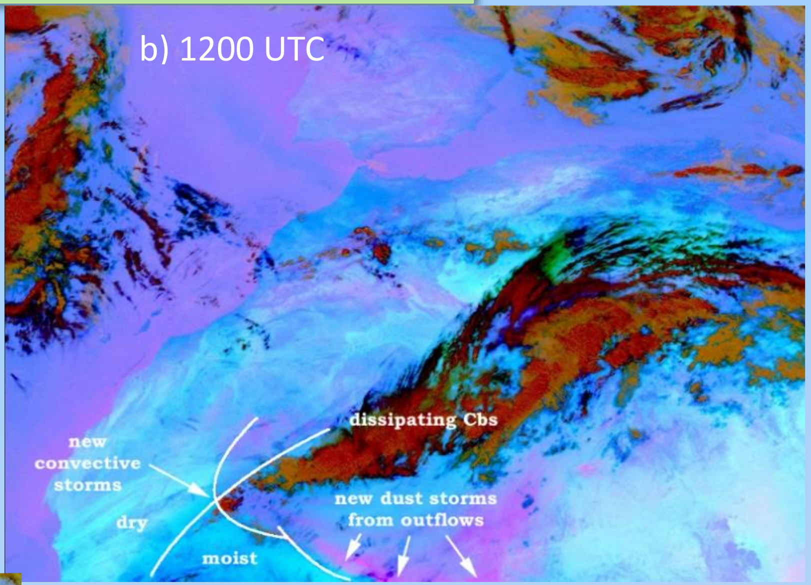

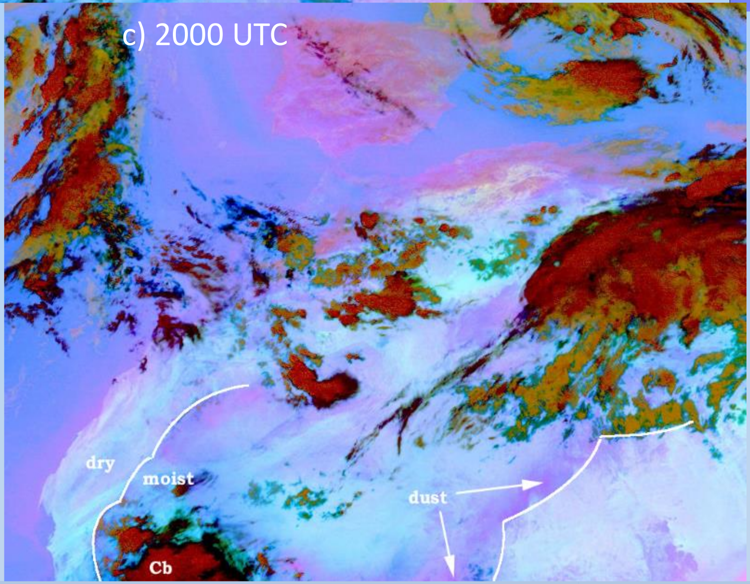

Figure 6.20. Same as Figure 6.19, except from 5 October 2005 at a) 0500 UTC, b) 1200 UTC, and c) 2000 UTC. (Source: EUMETSAT web site, 2014)

Copyright © 2016 John Wiley & Sons

African Monsoon Multidisciplinary Analysis

Chapter 6: *Nowcasting* – Authors: Rita D. Roberts and James W. Wilson

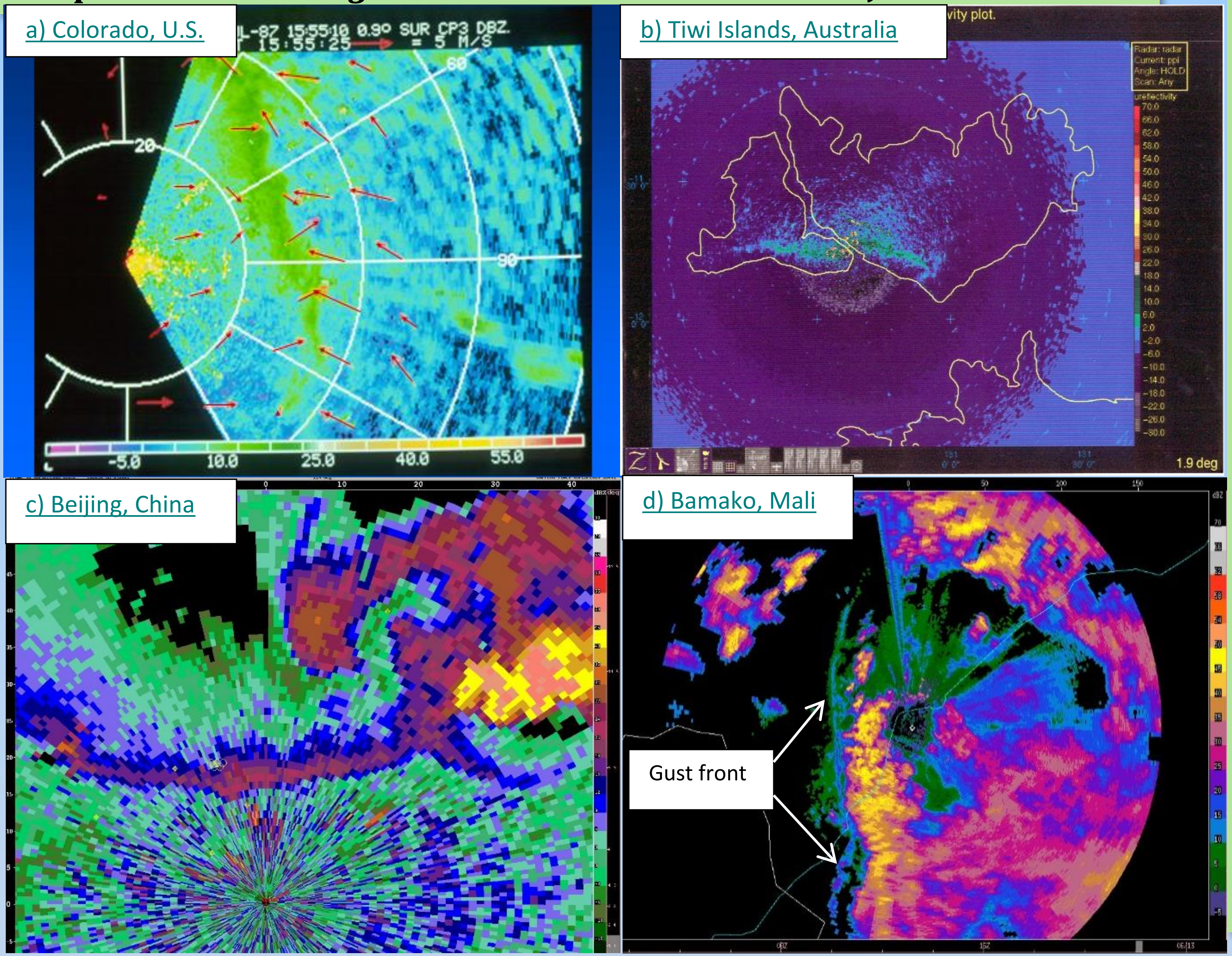

Figure 6.21. Examples of boundary-layer convergence lines ("boundaries") seen as thin lines of enhanced radar reflectivity. a) result of topographical-induced convergence, Colorado, United States, the red arrows are surface-wind vectors from surface mesonet stations b) sea-breeze front, Tiwi Islands off the north coast of Australia, c) gust front, Beijing, China during the Olympic Games, d) gust front at the leading edge of a squall line in Bamako, Mali, West Africa. (Source: J. Wilson, 2014)

Copyright © 2016 John Wiley & Sons

Chapter 6: *Nowcasting* – Authors: Rita D. Roberts and James W. Wilson

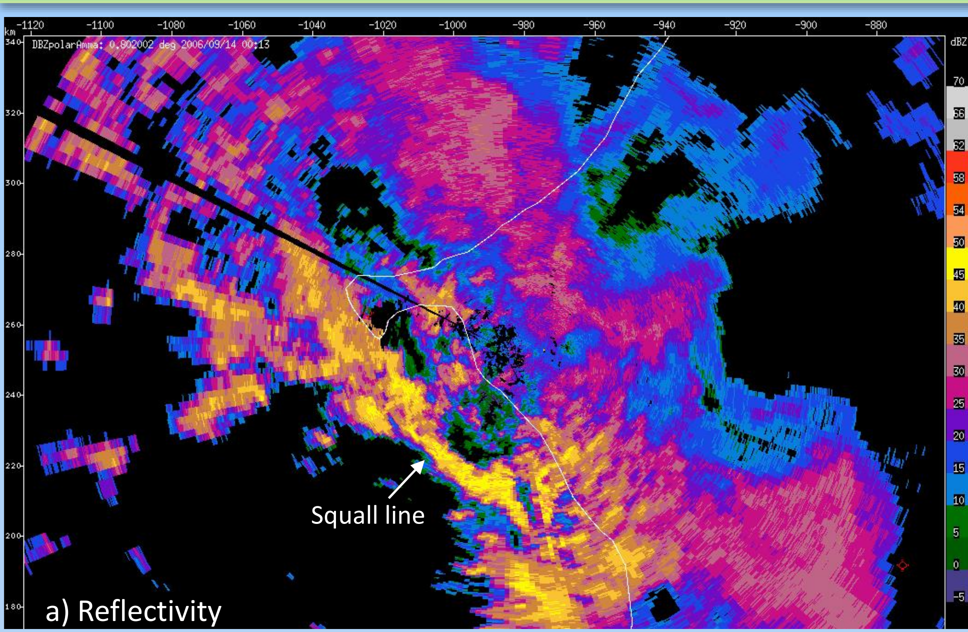

Figure 6.22. NASA NPOL detection of a) squall line (reflectivity in dBZ) and b) associated gust front (radial velocity in ms-1) near the Léopold Sédar Senghor International Airport in Dakaron 14 September 2006 at 0013 UTC. (Source: R. Roberts, 2014)

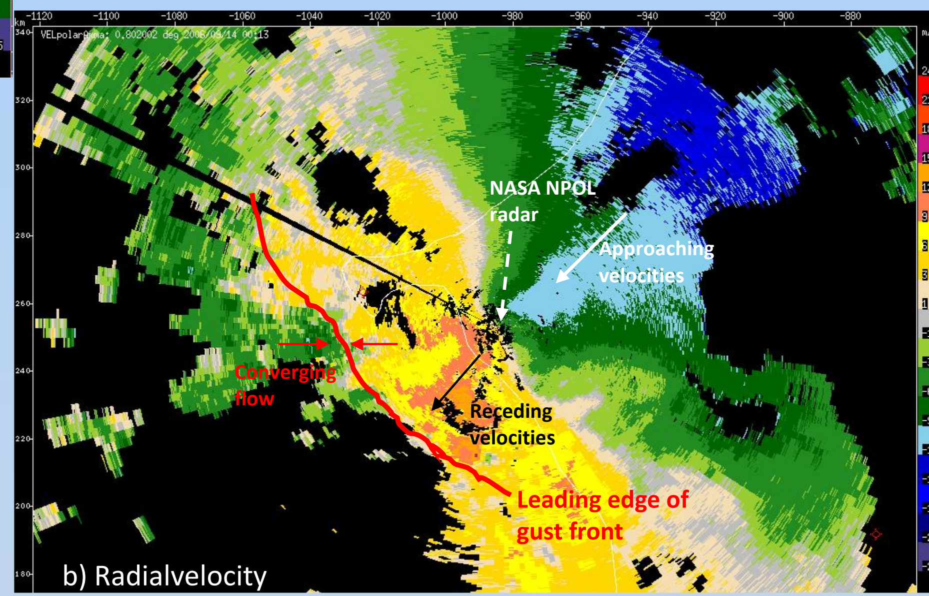

Copyright © 2016 John Wiley & Sons

African Monsoon Multidisciplinary Analysis

ACMAD

WMO

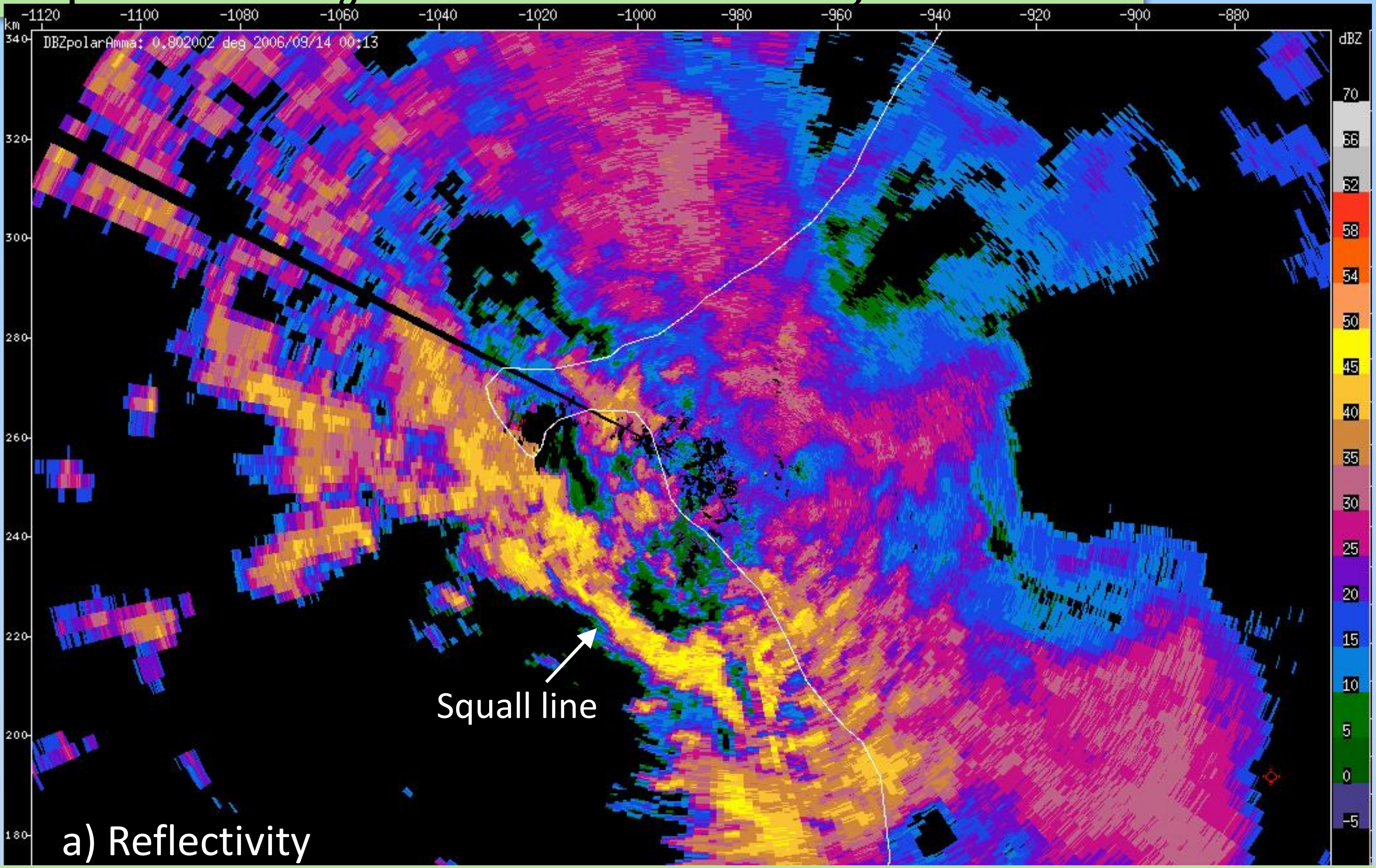

Figure 6.22. NASA NPOL detection of a) squall line (reflectivity in dBZ) near the Léopold Sédar Senghor International Airport in Dakaron 14 September 2006 at 0013 UTC. (Source: R. Roberts, 2014)

Copyright © 2016 John Wiley & Sons

Chapter 6: *Nowcasting* – Authors: Rita D. Roberts and James W. Wilson

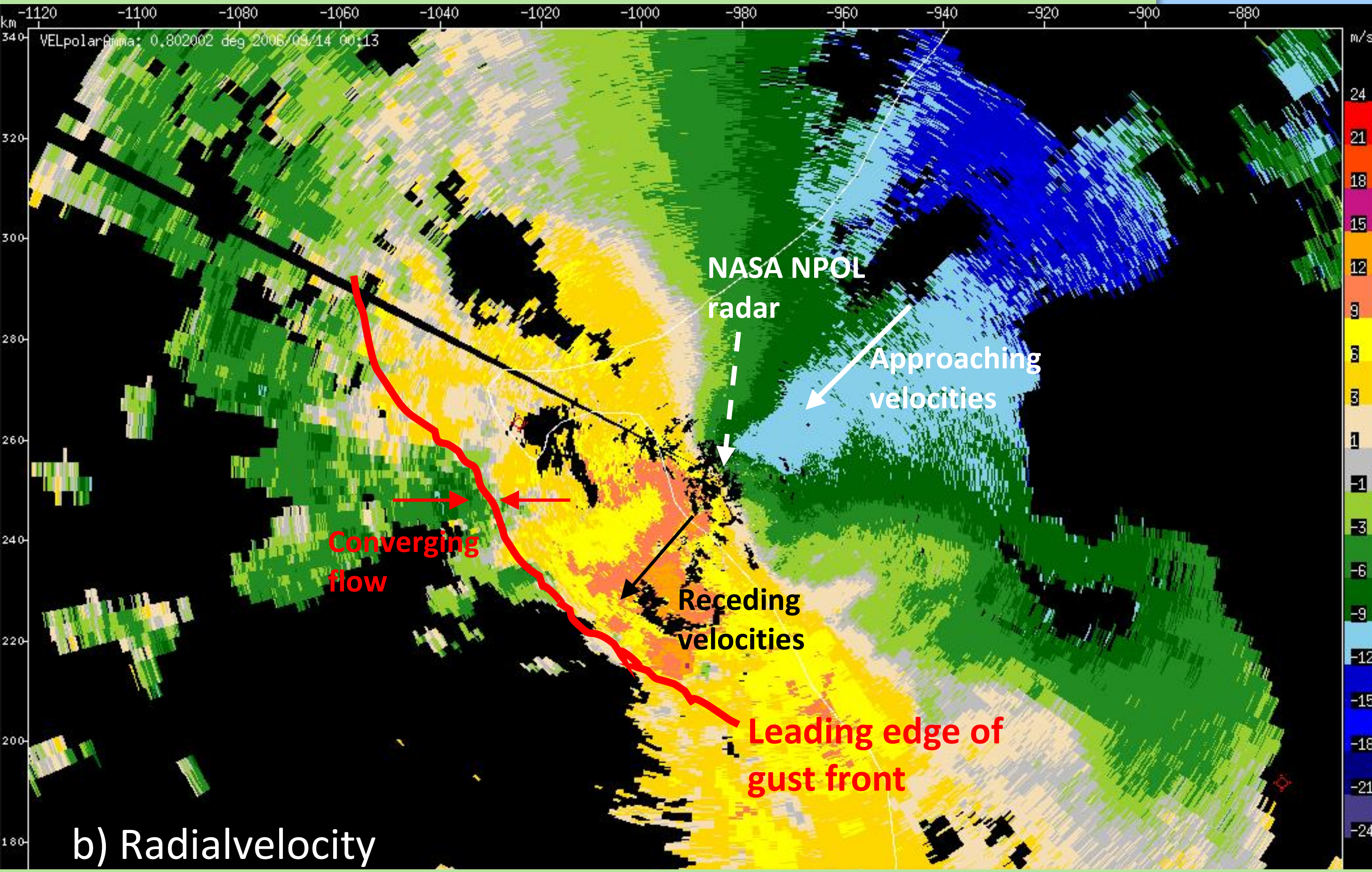

Figure 6.22. NASA NPOL detection of b) associated gust front (radial velocity in ms-1) near the Léopold Sédar Senghor International Airport in Dakaron 14 September 2006 at 0013 UTC. (Source: R. Roberts, 2014)

Copyright © 2016 John Wiley & Sons

Chapter 6: *Nowcasting* – Authors: Rita D. Roberts and James W. Wilson

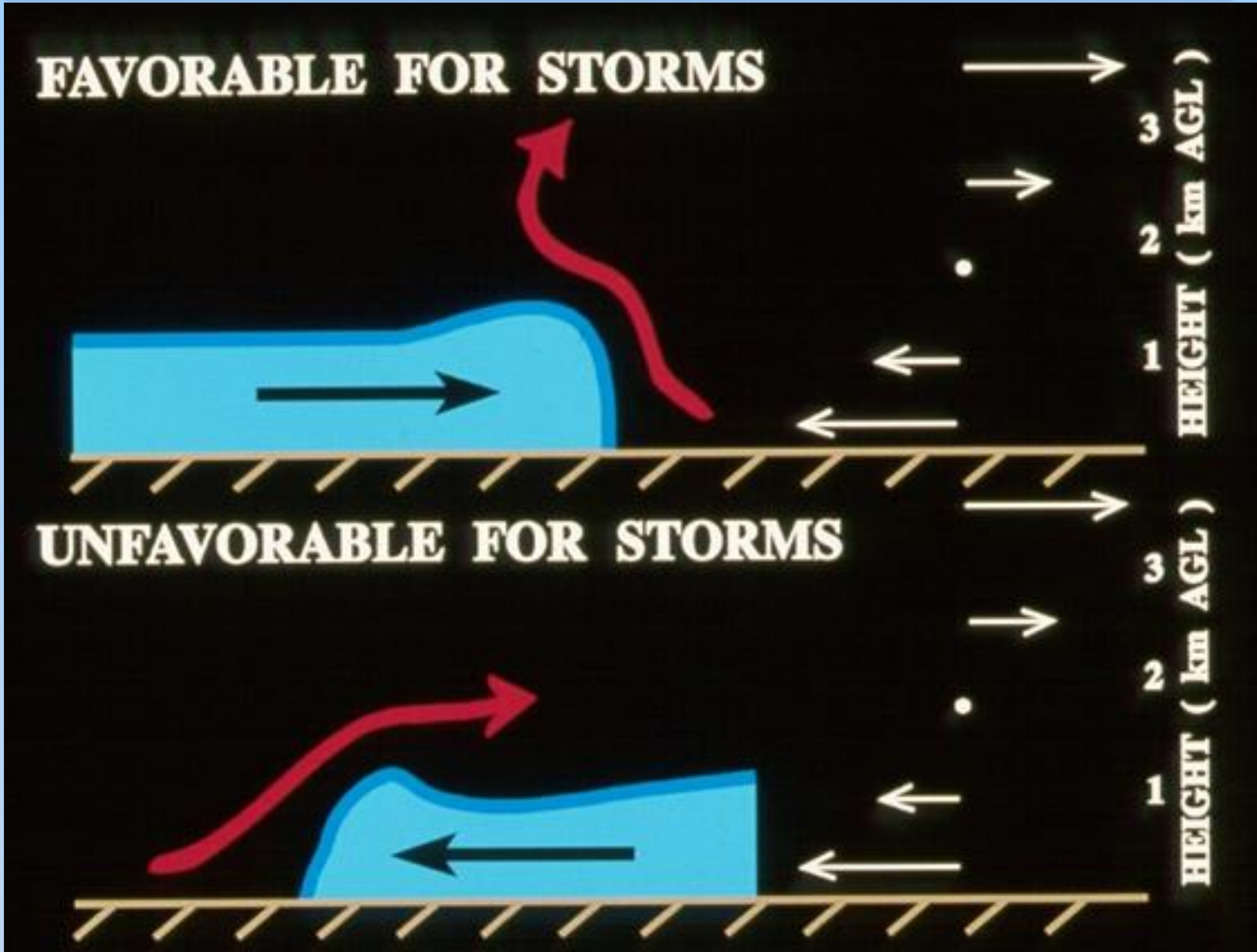

Figure 6.23. Illustration of favourable and unfavourable situations for convective storm development triggered by a convective storm outflow boundary. The red arrows show the airflow over the relative cool convective storm outflow (blue color). The black arrow shows the direction of motion of the outflow. The environmental winds are shown by the white vectors. This is an example for mid-level westerly winds. Similar plots can be made for mid-level easterlies. (Source: J. Wilson, 2014)

Copyright © 2016 John Wiley & Sons

African Monsoon Multidisciplinary Analysis

ACMAD

WMO

Chapter 6: *Nowcasting* – Authors: Rita D. Roberts and James W. Wilson

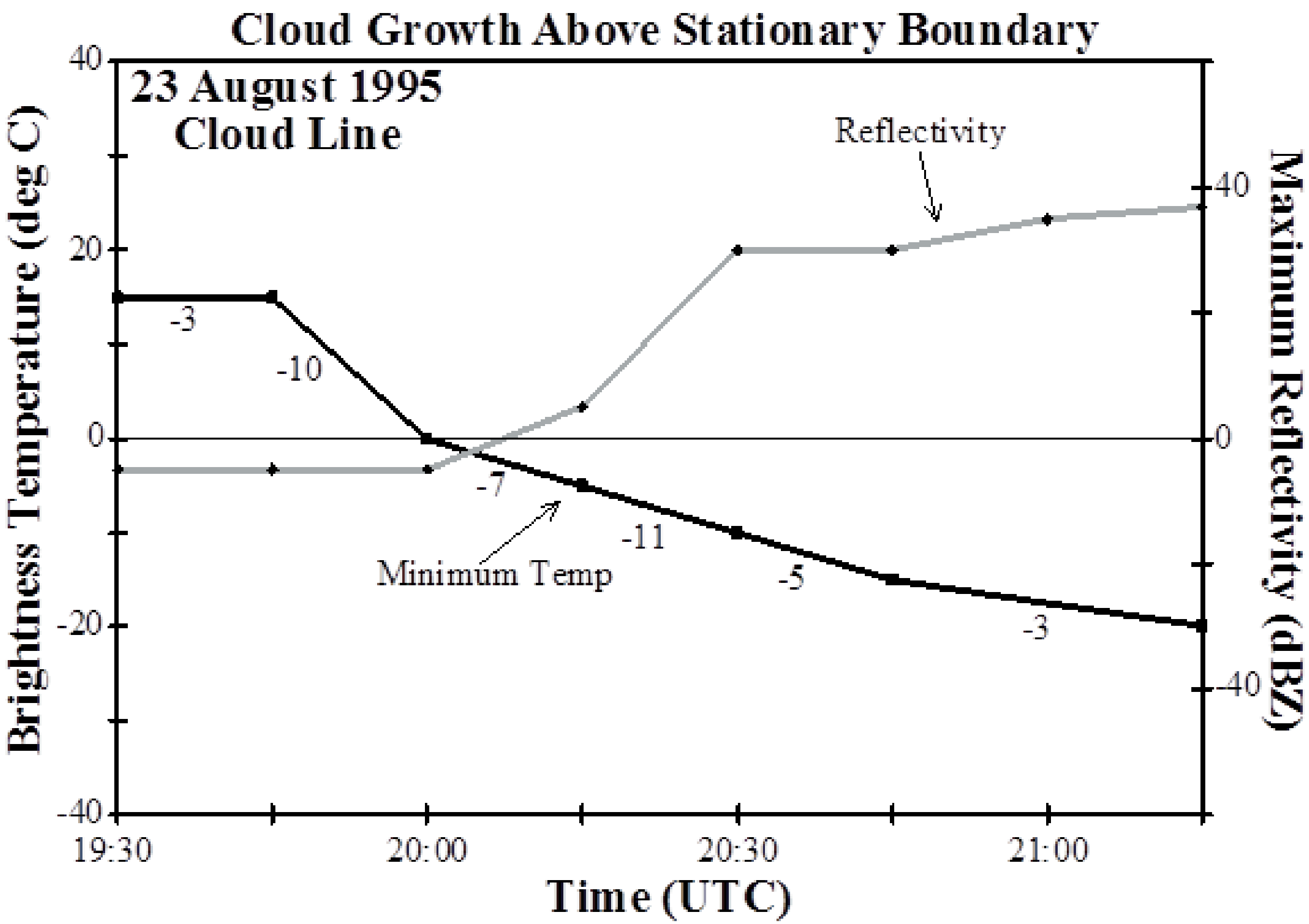

Figure 6.24. Time-series plot of minimum infrared (IR) brightness temperature (black curve) in °C and maximum radar reflectivity (grey curve) in dBZ associated with growth of a cloud line above a semi-stationary convergence line on 23 August 1995 in Colorado, USA. Rate of change values determined over 15 min intervals are listed below the temperature curve. (Source: Roberts and Rutledge, 2003)

Copyright © 2016 John Wiley & Sons

African Monsoon Multidisciplinary Analysis

ACMAD

WMO

Chapter 6: *Nowcasting* – Authors: Rita D. Roberts and James W. Wilson

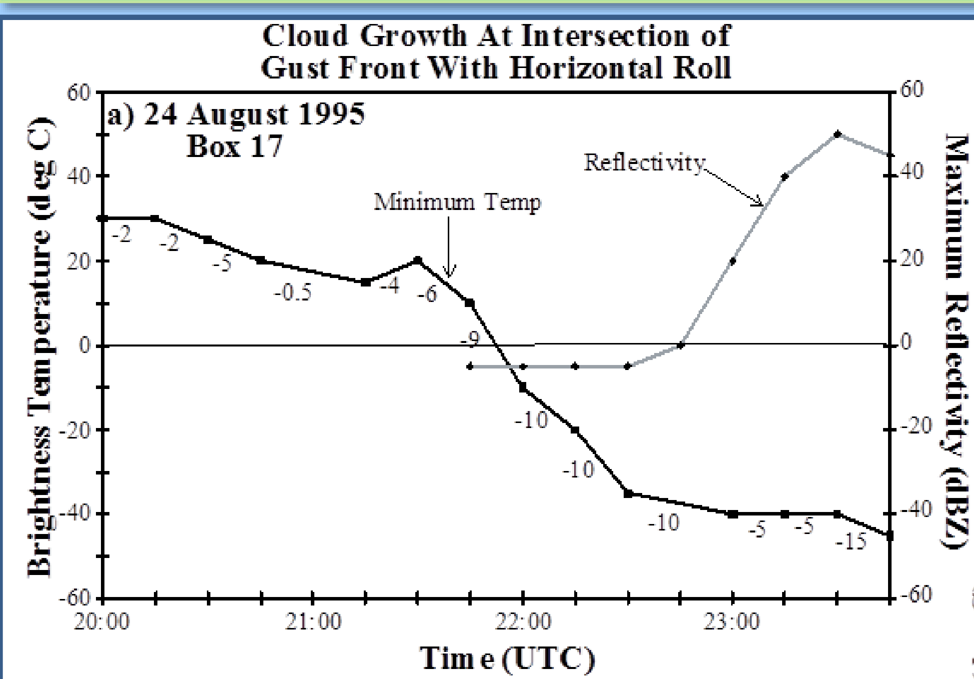

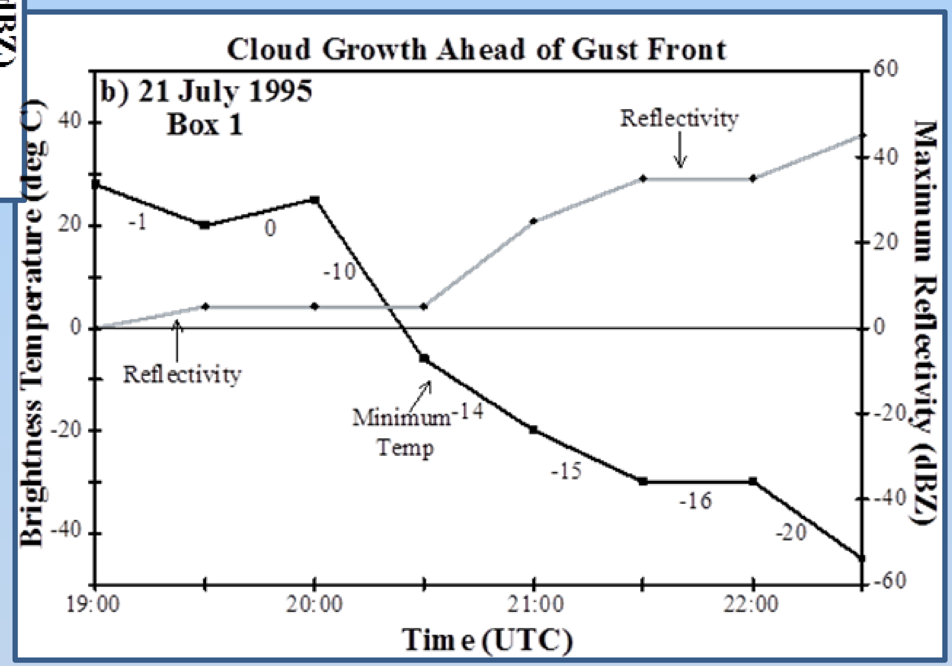

Figure 6.25. Same as Figure 6.24 but for (a) cloud growth above gust front interactions with horizontal rolls on 24 Aug 1995 and (b) cloud growth ahead of an approaching gust front on 21 Jul 1995. (Source: Roberts and Rutledge, 2003)

Copyright © 2016 John Wiley & Sons
African Monsoon Multidisciplinary Analysis
ACMAD
WMO

Chapter 6: *Nowcasting* – Authors: Rita D. Roberts and James W. Wilson

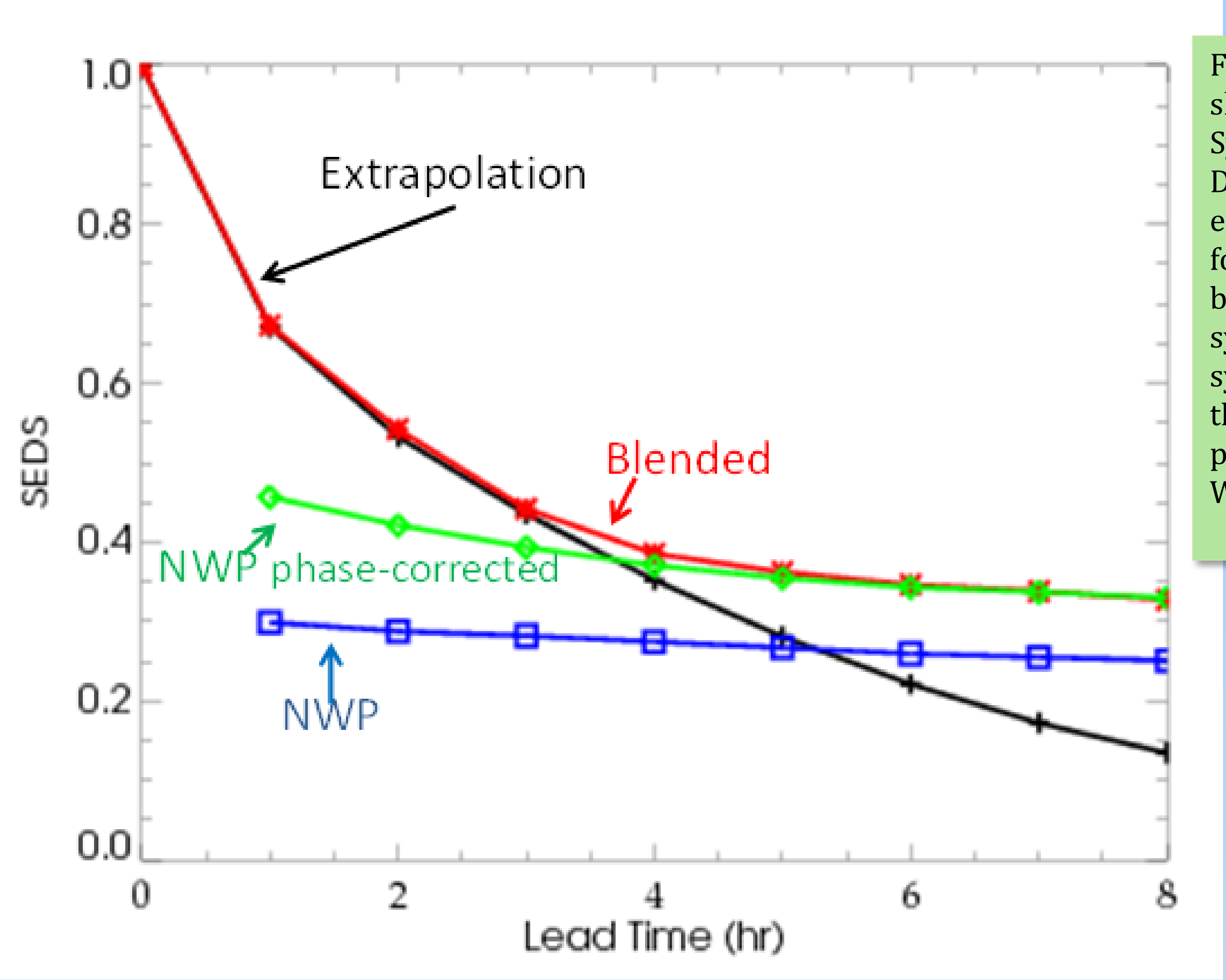

Figure 6.26. Example of skill score (SEDS, Symmetric Extreme Dependency Score, Hogan et al., 2009) versus forecast lead time for a blended nowcasting system. This blended system is being tested in the U.S. for aviation purposes. (Source: J. Wilson, 2014)

Copyright © 2016 John Wiley & Sons

Chapter 6: *Nowcasting* – Authors: Rita D. Roberts and James W. Wilson

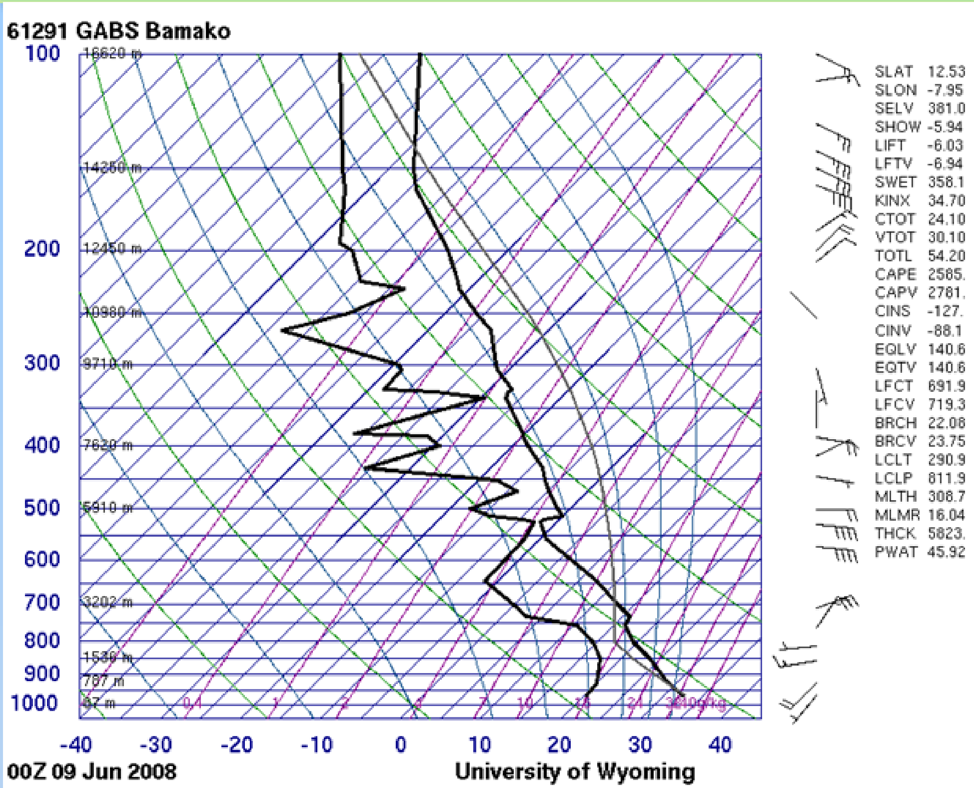

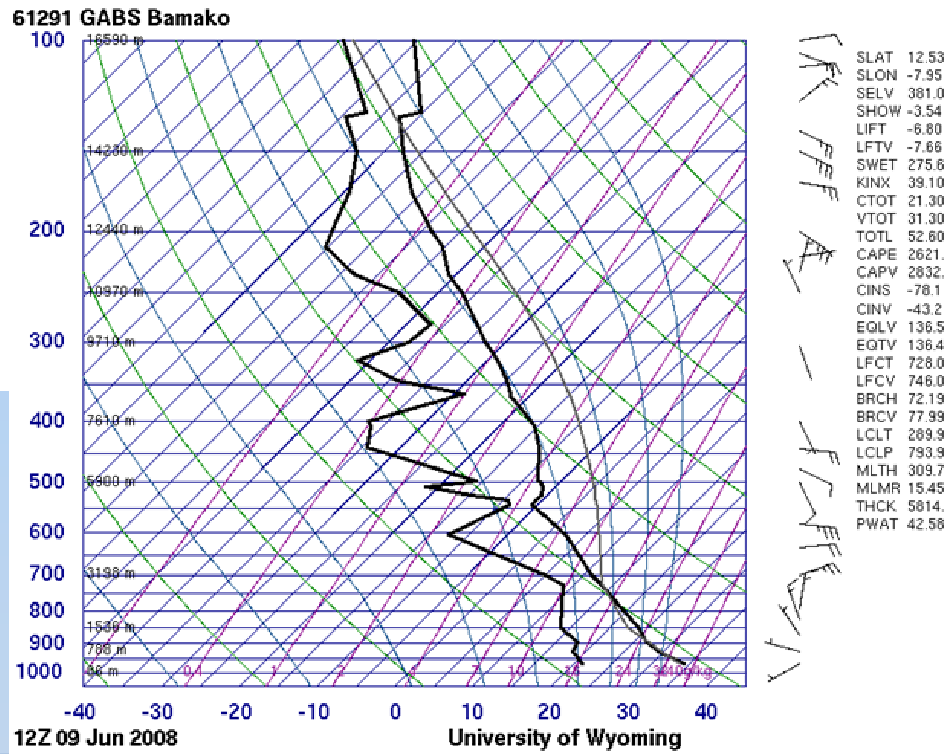

Figure 6.27. Bamako, Mali soundings from 9 June 2008 at 0000 UTC (top panel) and 1200 UTC (bottom panel) plotted on Skew-T plots. (Source: University of Wyoming web site, 2014)

Copyright © 2016 John Wiley & Sons

African Monsoon Multidisciplinary Analysis

ACMAD

WMO

Chapter 6: *Nowcasting* – Authors: Rita D. Roberts and James W. Wilson

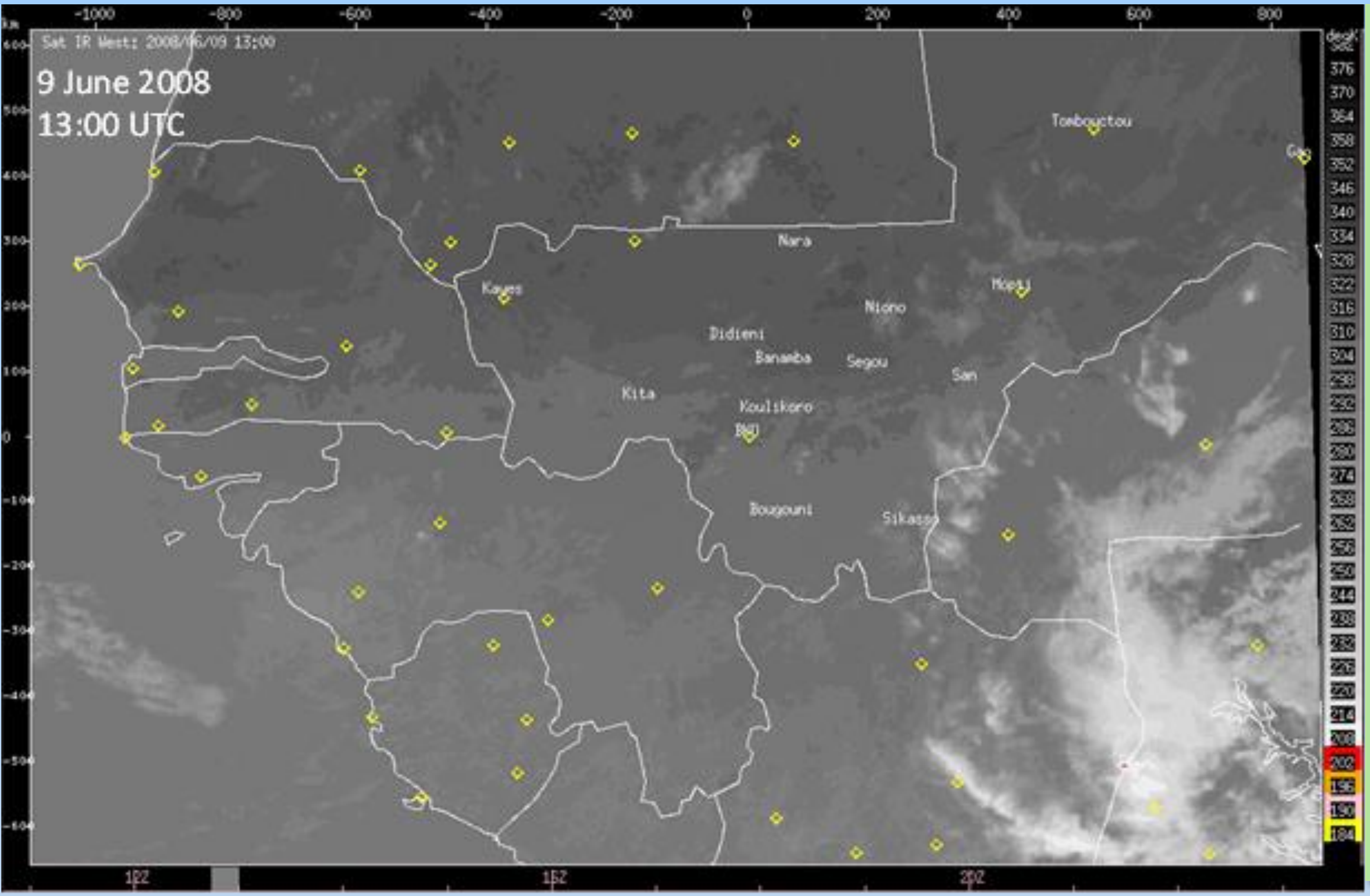

Figure 6.28. Satellite imagery of Infrared brightness temperatures at 13:00 UTC on 9 June 2008 for a portion of western Africa. Yellow diamond-shaped icons of the locations of major airports are overlaid and include the location of Bamako airport (BKO). White contours are country borders. (Source: R. Robert, 2014)

Copyright © 2016 John Wiley & Sons

African Monsoon Multidisciplinary Analysis

ACMAD

WMO

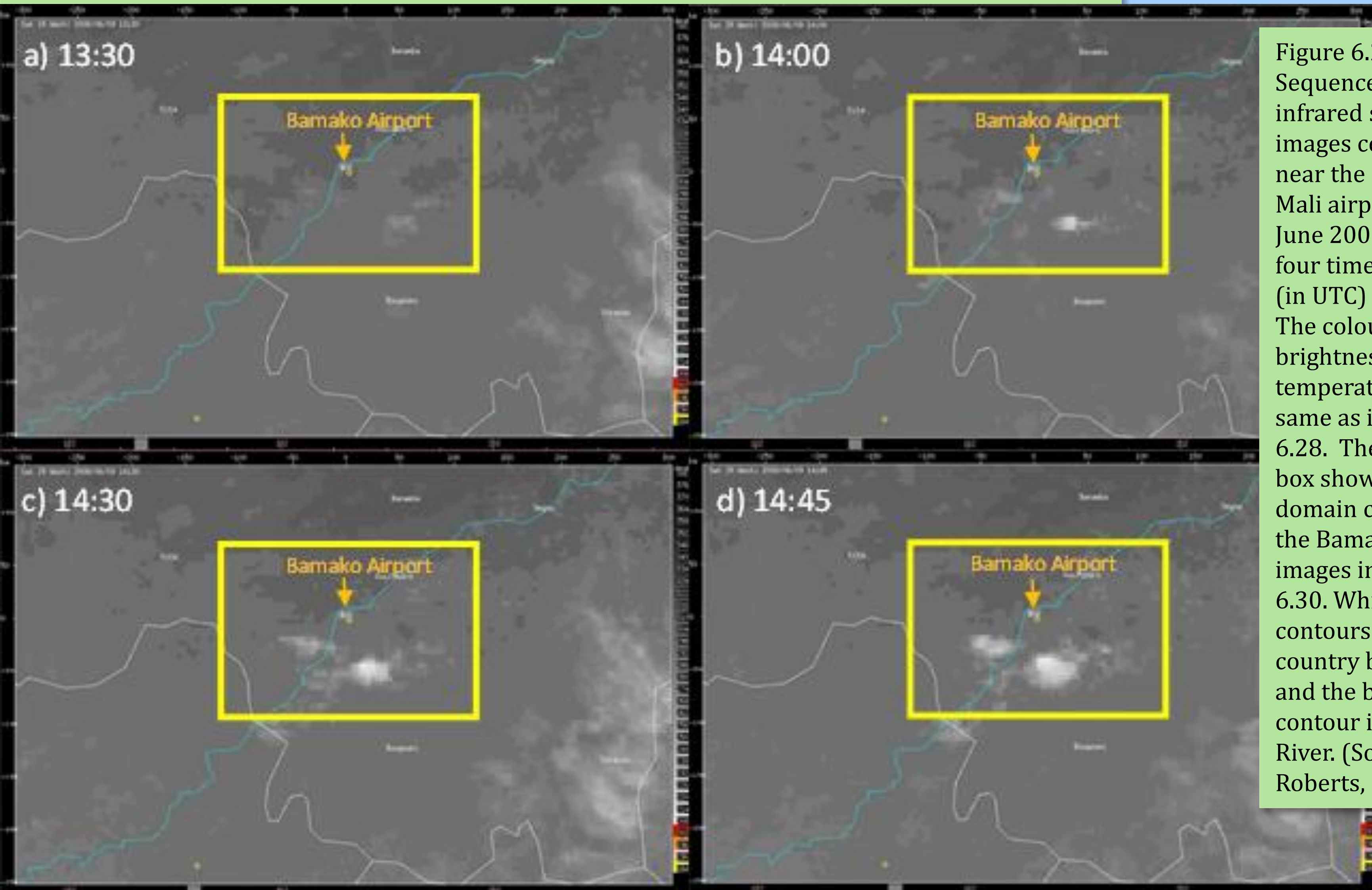

Figure 6.29. Sequence of infrared satellite images centered near the Bamako, Mali airport on 9 June 2008 at the four time periods (in UTC) shown. The colour scale, in brightness temperature, is the same as in Figure 6.28. The yellow box shows the domain covered by the Bamako radar images in Figure 6.30. White contours are country borders and the blue contour is the Niger River. (Source: R. Roberts, 2014)

Copyright © 2016 John Wiley & Sons

African Monsoon Multidisciplinary Analysis

ACMAD

WMO

Chapter 6: *Nowcasting* – Authors: Rita D. Roberts and James W. Wilson

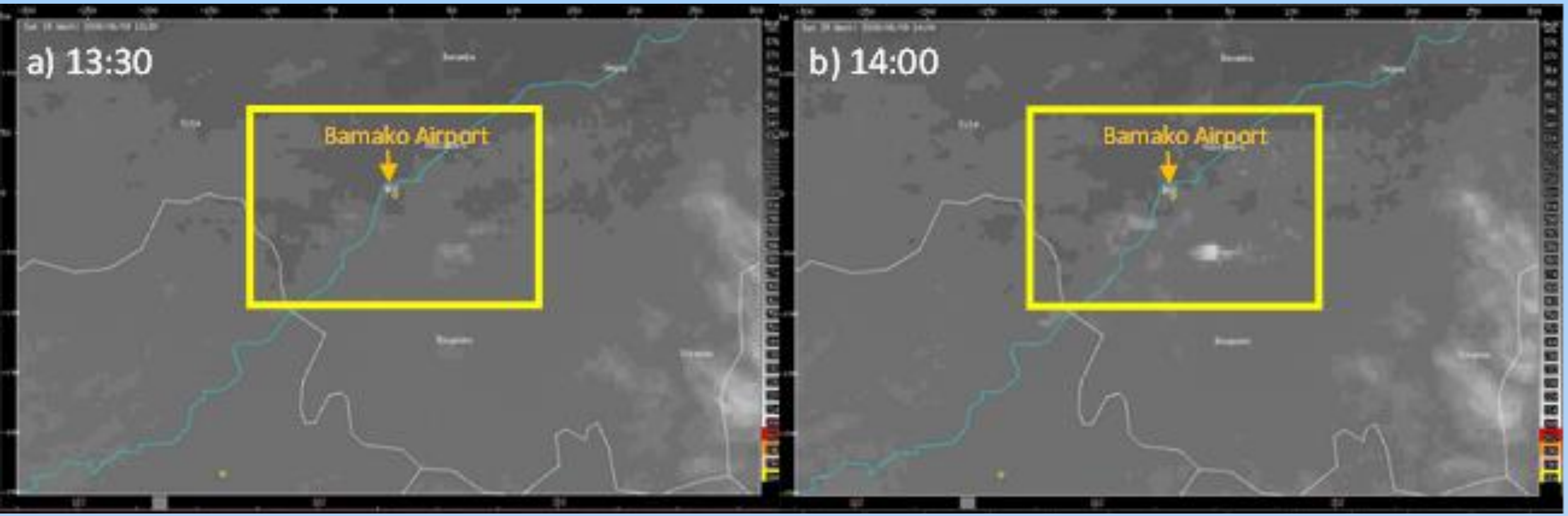

Figure 6.29. Sequence of infrared satellite images centered near the Bamako, Mali airport on 9 June 2008 at the four time periods (in UTC) shown. The colour scale, in brightness temperature, is the same as in Figure 6.28. The yellow box shows the domain covered by the Bamako radar images in Figure 6.30. White contours are country borders and the blue contour is the Niger River. (Source: R. Roberts, 2014)

Copyright © 2016 John Wiley & Sons

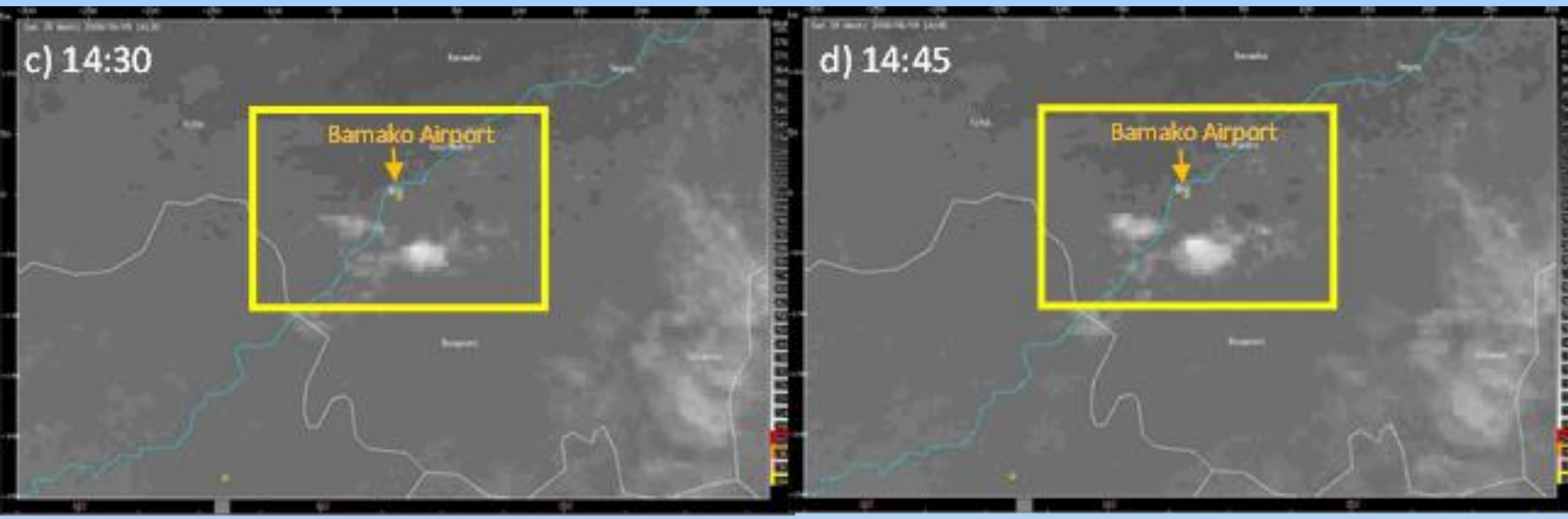

Figure 6.29. Sequence of infrared satellite images centered near the Bamako, Mali airport on 9 June 2008 at the four time periods (in UTC) shown. The colour scale, in brightness temperature, is the same as in Figure 6.28. The yellow box shows the domain covered by the Bamako radar images in Figure 6.30. White contours are country borders and the blue contour is the Niger River. (Source: R. Roberts, 2014)

Copyright © 2016 John Wiley & Sons